WN1316, A NOVEL ANTI-OXIDANT COMPOUND FOR THE TREATMENT OF LEBER'S HEREDITARY OPTIC NEUROPATHY (LHON)

Sohair Halas

A thesis is submitted to the

Faculty of Graduate and Postdoctoral Studies

in partial fulfillment of the requirements for the

MSc degree in Cellular and Molecular Medicine

Cellular and Molecular Medicine

Faculty of Medicine

University of Ottawa

ABSTRACT

Leber's Hereditary Optic Neuropathy (LHON) is a devastating mitochondrial disorder that leads to irreversible blindness. A mutation in the mitochondrial ND4 gene causes the majority of cases. Oxidative stress plays a role in disease pathology. WN1316 is a small molecule compound with potent anti-oxidant properties. Using *in vitro* and *in vivo* assays, the effectiveness of WN1316 in the treatment of LHON was tested. *In vitro,* the neuroprotective effects of WN1316 were tested against the oxidative stressors menadione and H2O2. These studies showed that WN1316 can protect SH-SY5Y neuronal cells and 661W photoreceptor-derived cells from oxidative stress in a concentration-dependent manner. Combination therapies with WN1316 and the X-linked Inhibitor of Apoptosis (XIAP) provided even better protection. *In vivo*, LHON disease had not progressed sufficiently to assess WN1316 effects on retinal function and axon counts. However we saw some delay in disease progression in the WN1316 group using electron microscopy. These initial studies suggest that WN1316 will be effective in the treatment of LHON, but we need to increase the timeline for disease progression to see the full effects of the compound.

TABLE OF CONTENTS

LIST OF FIGURES

LIST OF ABBREVIATIONS

AAV	adeno-associated virus
ADP	adenosine diphosphate
ALS	amyotrophic lateral sclerosis
AOND-QSAR	anti-oxidative neuronal cell death-quantitative structure activity relationship
ARVO	Association for Research in Vision and Ophthalmology
ATP	adenosine triphosphate
BSA	bovine serum albumin
CoQ10	coenzyme Q10
ERG	electroretinography
EM	electron microscopy
ETC	electron transfer chain
GFP	green fluorescent protein
HO-1	heme oxygenase-1
H2O2	hydrogen peroxide
IL-1 β	interleukin-1 β
INL	inner nuclear layer
iNOS	inducible nitric oxide synthase
IPL	inner plexiform layer
LHON	Leber's Hereditary Optic Neuropathy
mtDNA	mitochondrial deoxyribonucleic acid

MTS	mitochondrial targeting sequence
NAIP	neuronal apoptosis inhibitory protein
NQO1	NAD(P)H dehydrogenase [quinone] 1
Nrf2	NF-E2-related factor2 - nuclear factor erythroid 2 related factor 2
OCT	optical coherence tomography
ONL	outer nuclear layer
OPL	outer plexiform layer
OXPHOS	oxidative phosphorylation
PERG	pattern electroretinography
RGCs	retinal ganglion cells
ROS	reactive oxygen species
Rbpms	RNA-binding protein with multiple splicing
RPE	retinal pigment epithelium
rRNA	ribosomal ribonucleic acid
STR	scotopic threshold response
TBS	tris-buffered saline
tRNA	transfer ribonucleic acid
WRPE	woodchuck hepatitis virus posttranscriptional regulatory element
XIAP	X-linked inhibitor of apoptosis

ACKNOWLEDGEMENTS

First of all I thank God for giving me the opportunity, the patience and the commitment to complete my studies in the Master's program. A very special thank you to my supervisor, Cathy. I would have never reached where I am now and achieved what I have without you being there every step of the way to support, teach, help and inspire me. You have always believed in me, which gave me the courage to continue. I want to thank you more than words can say. My deepest thanks to Adam Baker for his continuous support, patience and encouragement since my first day in the lab. Adam, you have always been there to listen, guide and support me, and you have made the lab a pleasant and an inspiring place to work. I would like to thank Dr. Pamela Lagali. Although it has been only a short time that I have gotten to know you, I have learned a lot from your wide experience and colossal knowledge and from the scientific discussions I have had with you. It was a sincere pleasure to have Dr. Stuart Coupland and Dr. Robert Korneluk as my thesis advisory committee members. Thank you both for your continual support and guidance on my project. Thank you to Sarah Wassmer for her great help and support. Dr. Wai Gin Fong, thanks for helping me with everything when I needed it, and for the comic relief you have provided to all of us in the lab. Thank you to Dr. Li Jun Fang for helping me a lot with animal dissections and preparing flatmounts. A very big and special thank you to Yves de Repentigny from Dr. Rashmi Kothary's group for his great and invaluable help in the preparation of sections - I have gained and learned a lot from you. Thank you to my friends, Mohammad Taha, Joelle and Nora; you have always been there for me whenever I needed you. For my lovely family, my mother, brothers and sisters, a very deep thank you to you all for your continuous encouragement and for giving me the confidence to continue in the path you know I deserve

and that I was destined for. My beloved sons, Kamel, Khaled, Saleem and Essam, without your existence in my life, and your love and understanding, I would not be able to be where I am today to help you to be proud of your mother.

CHAPTER 1- INTRODUCTION

Leber's Hereditary Optic Neuropathy (LHON) is a neurodegenerative, maternally inherited, mitochondrial retinal disorder that is characterized by rapid, painless, bilateral, acute or subacute central vision loss. LHON preferably affects males more than females and has variable penetrance, such that 50% of males and 10% of females that harbour the pathogenic mitochondrial DNA (mtDNA) mutations develop visual loss (Koilkonda, & Guy, 2010). These features of LHON remain unexplained and reinforce the complexity of the disease and that other genetic (nuclear or mitochondrial) or epigenetic factors play a role in the development of the disease.

There are no effective treatments for LHON and the mechanisms that lead from mutation to disease are poorly understood. However, studies suggest that oxidative stress is a major component of disease aetiology (Battisti et al., 2004) (discussed in more detail below). This thesis assesses the therapeutic potential of WN1316, a small molecule compound with potent anti-oxidant properties, in the treatment of LHON. *In vitro* and *in vivo* assays were developed to assess the effectiveness of WN1316 in protecting cells in the retina from undergoing degeneration.

1.1 The Retina

The vertebrate retina is a complex thin layer of tissue that lines the back of the eye and is responsible for the detection of light, for transforming the sensory input into an electrical signal, and for transmitting this information to the brain. The mammalian retina is composed of three layers of nerve cell bodies, the outer nuclear layer (ONL), the inner nuclear layer (INL), and the retinal ganglion cell layer, and of two layers of synapses, the

outer plexiform layer (OPL) and the inner plexiform layer (IPL) (Figure 1). The retinal pigment epithelium (RPE) is the only epithelial layer of the retina and lies adjacent to the ONL (Kolb 2003). This layer, while not involved in the detection and propagation of light, is responsible for maintenance and recycling of the cells of the ONL, for providing the chromophores required in the phototransduction cascade, for reducing light scatter and for only allowing the absorption of light at a specific wavelength (Webvision: http://webvision.med.utah.edu/). Beneath the retinal pigment epithelium is the choroid, which is the main blood supply for the outer retina.

The three neuronal layers of the retina each house specific cell types important in the propagation of a light signal. The outer nuclear layer (ONL) contains the cell bodies of the rod and cone photoreceptors. Rods mediate vision in dim light while cones, concentrated in the centre of the retina, the macula, are responsible for color vision and visual acuity. The response to light and the generation of an electrical signal is initiated in the rods and cones. The rods and cones synapse in the outer plexiform layer to horizontal cells and bipolar cells whose cell bodies lie in the inner nuclear layer (INL). In the inner plexiform layer, further synapses occur between the axons of bipolar cells and the dendrites of ganglion cells, to continue propagation of the signal. Amacrine cells, located in the INL and the RGC layer, act to potentiate and integrate the ganglion cell signals. Ganglion cells represent the final output neurons of the vertebrate retina. Axonal projections of the retinal ganglion cells (RGCs) form the optic nerve and transmit the retinal signal into the brain visual centres for image interpretation (Webvision: http://webvision.med.utah.edu/). In LHON, it is predominantly

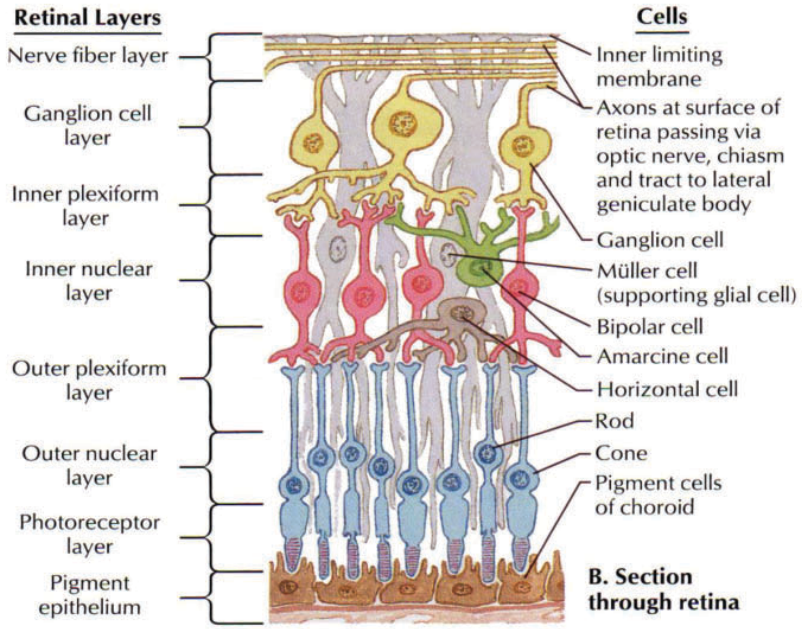

Figure 1: Structure of the mammalian retina. The retina is comprised of three main layers of neurons interconnected by synapses. Photoreceptor cells (rods and cones) are directly sensitive to light and are situated in the Outer Nuclear Layer (ONL). Photoreceptors synapse in the Outer Plexiform Layer (OPL) with bipolar cells and horizontal cells in the Inner Nuclear Layer (INL). In turn, bipolar cells synapse in the Inner Plexiform Layer (IPL) with retinal ganglion cells (RGCs) in the RGC layer. Amacrine cells in the INL help to refine the signal by connecting bipolar cells to retinal ganglion cells. RGCs send axonal projections through the optic nerve to the visual cortex in the brain. Figure is adapted from www.corpshumain.ca.

and specifically RGCs of the papillomacular bundle and their axons that undergo degeneration leading to irreversible central vision loss (Kirches, 2011).

1.2 Electrophysiology

Electroretinography is a valuable tool widely used in the laboratory and the clinic to assess retinal function and for the diagnosis of the diseased retina (Karanjia, ten Hove, & Coupland, S.G., 2011) The electroretinogram (ERG) involves brief flashes of light through the dilated pupil, which stimulate the different cell types of the retina. An electrical response is elicited and represented as a waveform whose components are derived from different cell types in the retinal circuitry. The response is recorded using electrodes that are placed on the cornea. For each component of the ERG waveform, two parameters are measured: the amplitude (in microvolts, μV) and the implicit time or latency (in milliseconds, ms). The amplitude measures the peak of the electrical response, while the latency represents the time it takes to reach the response amplitude (Webvision http://webvision.med.utah.edu/).

In the dark-adapted (scotopic) ERG, an intense brief flash of light causes a typical ERG trace, which consists of a hyperpolarizing, negative a-wave that is generated by photoreceptor cells and is the first to appear. The depolarizing positive b-wave follows, and is thought to originate from bipolar cells in combination with Muller glial cells. However, depending on the intensity of the light, different components of the ERG can be eliminated, and the function of specific cell types within the retina can be analyzed. For example, whereas an intense flash of light will produce both an a- and a b-wave, for weaker flashes of light, the a-wave is too small to be recorded and the b-wave will predominate (McCulloch et al., 2015). Moreover, very weak flashes of light in a dark-adapted animal will elicit a negative response which is opposite in polarity to the b-wave and is more sensitive than the

b-wave. This negative-going response is called the scotopic threshold response (STR), and it is thought to be indicative of inner retinal, and specifically RGC, function (Saszik, Robson, & Frishman, 2002). In the current study, we used the STR as a measure of RGC function to test the effects of disease progression and the effects of our therapy since RGCs are the cells most affected in LHON.

1.3 Leber's Hereditary Optic Neuropathy

1.3.1 – Genetics

In 1871, the German ophthalmologist Theodor Leber was the first to describe a group of patients, mostly male, presenting with a rapid onset hereditary optic neuropathy in their early decades of life (Levin, 2007) (Koilkonda, & Guy, 2010). The disease was subsequently named for him and came to be known as Leber's Hereditary Optic Neuropathy (LHON). After Leber's discovery, several pedigrees were described with a peculiar mode of transmission from a mother to an affected son or to a carrier daughter. The mode of inheritance of LHON was thought to be X-linked, but the knowledge that mitochondrial DNA (mtDNA) is maternally inherited led to the discovery of the first causative mtDNA point mutation linked to LHON.

The first causative mutation for LHON was discovered in 1988 and was reported to be a G to A transition at position 11778 of the mitochondrial genome (Wallace et al., 1988). This mutation resulted in an arginine to histidine substitution at amino acid position 340 in the mitochondrial NADH-ubiquinone oxidoreductase, subunit 4 (ND4) gene. More than 70% of cases of LHON are attributable to this mutation. Subsequently, LHON mutations were identified in multiple pedigrees at positions 3460 (ND1): (m.3460G>A/ND1) and

14484 (ND6): (m.14484T>CND6) of the mitochondrial genome. Collectively, these mutations account for 95% of all cases of LHON (Howell, 1997) (Guy et al., 2012).

1.3.2 Epidemiology and Clinical Manifestations

There are few epidemiological studies of LHON. However, in the North East of England a population-based study reported a minimum point prevalence to be 1 in 31,000 (Koilkonda, & Guy, 2010). Two comparable studies in The Netherlands and Finland suggested the incidence of visual failure secondary to LHON to be 1 in 39,000 and 1 in 50,000 respectively (Meyerson, Van Stavern, & McClelland, 2015). In Australia, 2% of individuals on the national blind registry were reported to be LHON patients. The relative frequency of the LHON-causing mutations differs throughout the world. Generally, the m.11778G>A variant is the most prevalent in Northern Europe, accounting for 70% of the cases. Among French Canadians, the m.14484T>C mutation is the most common (Yu-Wai-Man & Chinnery, 1993) (Yu-Wai-Man, Griffiths, & Chinnery, 2011).

As mentioned above, LHON is characterized by rapid, painless, bilateral loss of central vision leading to a central or centro-coecal scotoma that develops early in adult life. Individuals are completely asymptomatic prior to being suddenly affected in one eye, and within a few weeks to a few months, similar symptoms appear in the other eye. This sequential vision loss occurs in 75% of cases, with the remaining 25% of cases developing bilateral blindness at onset (Yu-Wai-Man & Chinnery, 1993). LHON patients suffer from severely reduced visual acuity and the fading of colors (dyschromatopsia). In the acute phase, ophthalmoscopic examination shows a characteristic appearance of optic nerve head swelling, edema of the peripapillary nerve fiber layer, telangiectatic microangiopathy and

vascular tortuosity. The chronic phase follows in which the optic disc becomes completely atrophic (Yu-Wai-Man & Chinnery, 1993).

The probability of visual improvement among LHON patients is infrequent and variant with the early age of onset being a favourable prognostic factor. Additionally, the causative mutation also has a role; the 11778/ND4 mutation has the worst recovery rate while patients with the 14484/ND6 mutation possess the highest recovery rate (Abu-Amero, 2011).

Although all cells in the body have the same mtDNA mutations, the striking feature of LHON is that retinal ganglion cells, the axons of which comprise the optic nerve, are the cells which are mostly vulnerable to cell death. Although several explanations have been proposed, the exact reason is not fully understood (Levin, 2007). Nevertheless, even though visual loss is the remarkable defining feature of this mitochondrial disorder, LHON is also less frequently associated with cardiac arrhythmias and neurological abnormalities such as peripheral neuropathy, postural tremor, cerebellar ataxia, multiple sclerosis-like syndrome and Parkinsonism with dystonia (Man, Turnbull, & Chinnery, 2002) (Nikoskelainen et al., 1995).

1.4 The Mitochondria

In order to understand the effects of mitochondrial mutations on LHON disease pathology, a brief understanding of mitochondrial structure and function is essential. Mitochondria are tubular shaped organelles that generate most of the cell's energy supply in the form of ATP (Figure 2A). They are unique in that they have their own genome. The mitochondrial genome is a circular, double-stranded molecule that is 16,569 bp long in vertebrates (Bibb, Van Etten, Wright, Walberg, & Clayton, 1981). It is a multi-copy genome

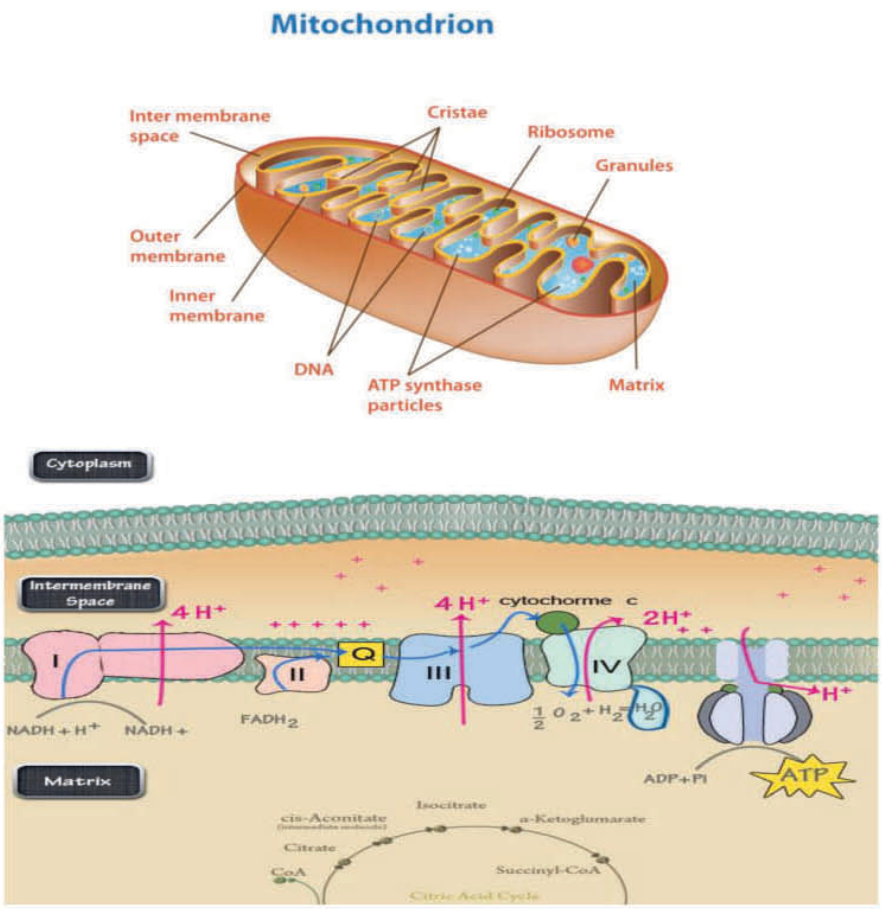

Figure 2. A) Mitochondria are the power houses of the cell. They are tubular shaped organelles that are bound by a highly specialized double-membrane system - the outer and the inner mitochondrial membranes. These two membranes define two mitochondrial compartments: the inter-membrane space and the inner mitochondrial matrix. Mitochondrial DNA is found in the matrix. The inner mitochondrial membrane is the site of the electron transport chain (ETC), which generates ATP through oxidative phosphorylation. The membrane is highly convoluted and folded into cristae. These convolutions increase the effective surface area reflecting the specific cellular ATP demand. Figure adapted from www.freelearningchannel.com. **Figure 2B. Oxidative Phosphorylation is the main pathway to generate most of the cellular energy in the form of ATP.** Complex I is one of five complexes that are large enzymes embedded in the inner mitochondrial membrane and are responsible for the transport of electrons. The electron transport is coupled with the pumping of hydrogen ions into the inner membrane space, which will create an electrochemical gradient across the membrane that will be utilized by ATP synthase (also referred to as Complex V) to generate ATP from ADP. Figure is adapted from www.premedhq.com.

consisting of hundreds to thousands of mtDNA molecules per cell depending on the energy demands of the cell. Mitochondrial DNA encodes 2 ribosomal RNAs (12S and 16S rRNA), 22 transfer RNAs (tRNA) and thirteen essential polypeptide subunits of the respiratory chain complexes. All the other subunits are encoded by the nuclear DNA, synthesized on cytoplasmic ribosomes then imported into the mitochondria and distributed to different compartments (inner and outer membrane, matrix and intermembrane space (Yu-Wai-Man, Griffiths, & Chinnery, 2011) (Anderson et al., 1981)

Mitochondria are bound by a highly specialized double-membrane system (Figure 2A). The two membranes enclose and define two mitochondrial compartments: the inter-membrane space and the inner mitochondrial matrix space. Each of these compartments plays distinct functional roles. However, the inner membrane and the matrix are considered the major working compartments of the mitochondrion. The inner mitochondrial membrane is highly convoluted and folded into cristae. These convolutions increase the effective surface area, reflecting the specific cellular ATP demand (Cooper, 2000). A number of highly specialized protein complexes are embedded in the inner mitochondrial membrane. These complexes are involved in electron transport and the generation of ATP through oxidative phosphorylation (Alberts et al., 2002) (Figure 2B).

1.4.1 Oxidative Phosphorylation

ATP is generated to meet the energy demands of the cell through glycolysis and oxidative phosphorylation. Glycolysis, the less efficient of the two processes, occurs in the cytoplasm. In the presence of oxygen, the products of glycolysis are then transported into the mitochondrial matrix, where they enter the Krebs (citric acid) cycle. Through a process

called oxidative phosphorylation, by-products of the Krebs cycle (NADH and FADH2) are then used by the electron transport chain embedded in the inner mitochondrial membrane to generate most of the ATP required by the cell.

The electron transport chain (ETC) is composed of 4 major complexes (Complexes I, II, III and IV) and ATP synthase (sometimes referred to as Complex V) (Figure 2B). NADH and FADH2 are oxidized by donating electrons to the first two complexes in the ETC. The high-energy electrons are transferred along the complexes of the ETC in an efficient and tightly regulated manner. A number of molecules such as ubiquinone (coenzyme Q10) also have a unique role in the transfer of electrons. The process of transfer of electrons across the complexes of the ETC releases a high amount of energy that is used to pump protons across the inner membrane (from the matrix to the inter-membrane space). This creates an electrochemical gradient across the inner membrane that is finally used by Complex V or ATP synthase to convert ADP to ATP. The ND1, ND4 and ND6 genes that carry the LHON mutations are all subunits of Complex I of the ETC, leading to the belief that these mutations lead to disease by affecting ATP production in the cell (Saraste, 1999) (Papa et al., 2011) (Mailloux & Harper, 2012) (Lenaz, 2012).

1.5 LHON Genetics

1.5.1 Homoplasmy and Heteroplasmy

Different cells in the body contain variable numbers of mitochondria ranging between 100-10,000, and each mitochondrion harbours 2-10 mtDNA molecules. This indicates that the copy number of mtDNA is extremely high and distributed heterogeneously depending on tissue-specific energy needs. When all the mtDNA content of the cell is either completely

wild-type or completely mutant, the cell is then in a homoplasmic condition. However, when there is a mixture of mutant and wild-type mtDNA, this is called heteroplasmy (Yu-Wai-Man, Griffiths, & Chinnery, 2011). Pathogenic mtDNA mutations of most LHON patients are homoplasmic although there is a small percentage of individuals that carry heteroplasmic mutations. The pattern of mutation (either homoplasmy or heteroplasmy) does not affect the clinical manifestation of the disease (Koilkonda, & Guy, 2010)

1.5.2 Disease Association with a Particular Haplotype

There is evidence that the mitochondrial DNA background is an important genetic determinant that influences the phenotype of mitochondrial disease. Mitochondrial DNA is highly polymorphic. During human evolution, a number of mitochondrial sequence variants have become fixed in certain populations and accumulated following human migration. The mitochondrial DNA haplogroup is a combination of alleles at different chromosomes that are closely linked and inherited together. There are 18 mitochondrial DNA haplogroups identified in the human phylogenetic tree. The mtDNA haplotypes have an impact on the phenotypic expression of LHON. Several studies have confirmed the strong association between mtDNA haplotypes of haplogroup J with two out of three primary causative mutations in LHON, m.14484T>C and m.11778G>A, but not m.3460G>A, further confirming that the mtDNA background can modulate disease penetrance (Man et al., 2004). The haplogroup J increases the risk and severity of the visual loss in LHON. Secondary mutations, which are also detected in unaffected control individuals, increase the severity of LHON. Although secondary mtDNA mutations do not alter evolutionarily conserved amino

acids, they may play a synergistic role in the severity of phenotypic expression of LHON (Koilkonda, & Guy, 2010).

1.5.3 Penetrance, Risk Factors and Age of Onset

Regardless of the haplogroup, or the heteroplasmic or homoplasmic state of the mtDNA mutations, only some individuals will develop the disease, indicating that other genetic or environmental factors may have a triggering role in LHON pathogenesis. Male predominance and incomplete penetrance remain the two unexplained issues in LHON. Mitochondrial biogenesis (the formation of new mitochondria) may offer one explanation. Studies on different experimental systems (blood cells or skin-derived fibroblasts) have shown that having higher mtDNA copy number by increasing mitochondrial biogenesis can overcome the pathogenic effects of mtDNA mutations. Estrogens can activate mitochondrial biogenesis and thus females may be better protected against mitochondrial dysfunction (Pisano et al., 2015).

Additional risk factors for the development of LHON are cigarette smoking, alcohol consumption, chemical toxins, psychological stress and anti-retroviral and anti-tuberculosis drugs. A recent study by Giordano et al (2015) showed that in white blood cells and in skin-derived fibroblasts of LHON patients, cigarette derivatives could significantly decrease mtDNA copy number and oxidative phosphorylation (OXPHOS) (Giordano et al., 2015).

There are additional inexplicable factors associated with the development of LHON. Firstly, it is difficult to explain why the disease arises at a particular age (second or third decade of life) given that the causative mutations are present at birth. Secondly, after the disease onset, it is not clear why in most cases one eye is affected first and then the other eye

becomes involved a short time thereafter. Thirdly, LHON has a specific type of visual field defect (cecocentral scotoma), in which the visual loss is extended from the central visual field to the natural blind spot, while other optic neuropathies exhibit a common central scotoma. Lastly, some LHON individuals show spontaneous recovery that may occur a long time after disease onset while others do not (Levin, 2007)

1.6 Mechanisms of Cell Death in LHON

1.6.1 Oxidative Stress and Generation of Reactive Oxygen Species (ROS)

Oxidative phosphorylation (OXPHOS) is a vital cellular process that leads ultimately to the production of ATP. However, during the transport of electrons in the ETC, electron leakage can occur resulting in the generation of reactive oxygen species (ROS) (Lenaz, 2012) (West, Shadel, & Ghosh, 2011). ROS production and altered ATP generation are two major pathways involved in LHON pathology and in the consequent and particular susceptibility of RGCs to apoptotic cell death. Since all LHON mutations cause substitutions of amino acids in NADH-ubiquinone oxidoreductase (Complex I of the ETC), the most prominent effect is a decrease in complex I activity leading to apoptotic cell death of RGCs.

Importantly, our understanding of LHON pathogenic mutations and their biochemical effects has been obtained through the study of transmitochondrial cytoplasmic hybrids (cybrids) in human cell lines. These cells were generated by the fusion of two cell types, with the mitochondria derived from one cell type and the nucleus and other cytoplasmic organelles derived from the other cell type. For this purpose, osteosarcoma cells depleted of their mtDNA were fused with enucleated cells (usually platelets) from LHON donors to produce cybrids carrying LHON mutant mitochondria (Levin, 2007). Cybrid studies showed

that LHON mutations caused reductions in oxygen consumption and respiration rates. LHON cybrids grown in glucose-deficient galactose media were forced to rely on OXPHOS solely as a primary energy source rather than glycolysis. Under these restrictive conditions, these cell lines, with mutated mitochondria, experienced apoptotic cell death in a Fas-dependent manner (Danielson et al., 2002). In contrast, another study using the same glucose-deficient galactose media suggested that cell death in cybrids occurred in a caspase-independent manner (Zanna et al., 2005). In addition, cybrid studies have shown that LHON cells have increased ROS production, increased sensitivity to hydrogen peroxide production and enhanced sensitivity to oxidative stress (OS) (Yu-Wai-Man, Griffiths, & Chinnery, 2011). Although the use of cybrid lines has been useful in providing insights into LHON pathology, these studies are still restricted because of the problem of using tumor cells to represent neuronal cells for the study of defective neuronal energy metabolism. Besides the fact that neurons use OXPHOS for the production of energy and tumor cells use glycolysis, the latter cells are also genetically heterogeneous and may have acquired chromosomal aberrations. Thus, understanding mechanisms of LHON pathology through the study of cybrids can result in misleading conclusions on the effects of mitochondrial mutations (Ghelli et al., 2003) (Levin, 2007) (Kirches, 2011).

1.6.2 Greater Vulnerability of Retinal Ganglion Cells (RGCs)

One of the most striking features of LHON is that although mitochondrial DNA mutations are present in all retinal cell types, it is only RGCs of the papillomacular bundle region of the retina that selectively undergo degeneration. The factors that spare other cell types such as photoreceptors and the retinal pigment epithelium, and contribute to the greater

susceptibility of RGCs to cell death are not fully understood. Some studies reported that this might be in part due to the high energy requirements for axonal transport along the long axons of the RGCs. The two motor proteins responsible for axonal transport, dynein and kinesin, require large amounts of energy to perform their function. Mitochondrial dysfunction results in reduction of ATP synthesis, which contributes to disruption of axonal transport, RGC degeneration and visual loss (Koilkonda, & Guy, 2010).

Certain aspects of the anatomy of the optic nerve, which houses the axons of the RGCs, could affect and worsen the pathological consequences of LHON mutations. The lamina cribrosa is a mesh-like structure that allows passage of the axons of the optic nerve through the sclera. RGCs axons acquire myelination only in the post-laminar region, and are unmyelinated in the pre-laminar segment. Generation and propagation of an action potential is a process that requires high amounts of energy. Thus, it is less efficient in the pre-laminar unmyelinated axons. Histological studies in normal human optic nerves revealed that the mitochondrial content differs greatly between the pre- and post- laminar regions. In the absence of myelination in the pre-laminar space, there is an increased mitochondrial content compared with the post-laminar region, reflecting the higher energy demands for nerve conduction in the unmyelinated axons. Therefore, the impairment of energy that is resulting from LHON mutations will have worse consequences in the vulnerable pre-laminar segment of the optic nerve. Another important factor is that the papillomacular bundle region of the retina contains parvocellular RGCs that have much smaller cross-sectional areas compared to larger magnocellular RGCs, which might contribute to specific cell death within this region resulting in central vision loss (Yu-Wai-Man, Griffiths, & Chinnery, 2011).

A study of oxidative stress in the RGC-5 cell line suggested that RGCs have a particular cell type-specific susceptibility to the effects of complex I mutations, which are the primary mutations in LHON disease. In this study, it was found that RGCs produce superoxide at much lower levels than other brain neuronal cell lines, and it was hypothesized that RGCs regulate superoxide in a different way compared with other neuronal cells (Levin, 2007). LHON mtDNA mutations increase superoxide production rates and interfere with its regulation, which triggers an aberrant apoptotic cascade. RGCs are more sensitive and need tighter regulation of superoxide, which is more tolerated by other neuronal cells (Levin, 2007). There is a caveat to these studies, however. More recent work suggests that the RGC-5 cell line is not in fact composed entirely of retinal ganglion cells and is contaminated with 661W photoreceptors cells (Van Bergen et al., 2009) (Krishnamoorthy, Clark, Daudt, Vishwanatha, & Yorio, 2013). Consequently, the studies on superoxide in these cells may not reflect what is happening in RGCs *in vivo*. However, *in vivo* studies also suggest that RGCs in particular use superoxide intracellularly to regulate apoptosis after axonal injury. Superoxide is produced mainly by complexes I and III of the electron transport chain. Since mtDNA mutations in LHON affect mainly ETC complexes and result in aberrant superoxide production, this may explain the specific RGCs death since these cells need tighter regulation of superoxide production and are less tolerant to the consequences of aberrant superoxide generation and aberrant apoptosis signalling (Levin, 2007).

1.7 Current Therapies for LHON

There is no effective treatment for LHON to date and the currently available therapies have been limited and only supportive. Idebenone, a short chain derivative of coenzyme Q_{10}

(CoQ_{10}), is the only agent used for the treatment of LHON. CoQ_{10} is a component of the electron transport chain (ETC) that plays a central role in electron transfer and generation of cellular ATP. It also serves to increase cellular anti-oxidant defenses. Studies have shown that a combination of idebenone and its derivatives with vitamin B2 and vitamin C can be effective, although not in all patients. Treatment outcomes are variable among patients, depending on the causative mutation and the degree of disease progression at the time that therapy is initiated (Sadun, La Morgia, & Carelli, 2011) (Koilkonda, & Guy, 2010).

1.8 Animal Models of LHON

Effective treatment strategies for LHON remain elusive. This is due to the fact that although the causative mutations are identified, the pathogenic mechanisms leading from gene mutations to retinal ganglion cell and optic nerve degeneration and subsequent blindness are not fully understood. An important reason for the poor understanding of the linkage between the causative mutation and manifestation of the disease is the lack of reliable animal models that recapitulate LHON and would enable investigating the pathogenesis of optic neuropathies and testing effective targeted therapeutic approaches (Yu et al., 2012). It is difficult to introduce mutations into the mouse mitochondrial genome in a live animal; this is because most of the mitochondrial mutations that affect complex I activity lead to a lethal phenotype and because it is difficult to target mtDNA due to the large number of copies of DNA per mitochondrion and the large number of mitochondria per cell. However, in 2007, a mouse model of LHON was produced using an adeno-associated virus (AAV) to deliver mutant ND4 directly to the retina with an intravitreal injection (Qi, Sun, Lewin, Hauswirth, & Guy, 2007). In this model, mutant ND4, which would normally be transcribed in the

mitochondria, was allotopically expressed using the nuclear machinery. The resulting protein was fused to a mitochondrial targeting sequence and imported into the mitochondria. The authors showed that the mutant ND4 replicated LHON in mice by causing increased levels of reactive oxygen species, optic nerve head swelling and apoptotic death of retinal ganglion cells (Qi, Sun, Lewin, Hauswirth, & Guy, 2007).

In order to develop a model that better reflected the disease in humans, Yu et al. (2012) developed an AAV system that had a mitochondrial targeting sequence in the viral capsid and would be imported into the mitochondria to allow transcription of the mutant ND4 in its natural environment. The authors reported reductions in retinal function using Pattern Electroretinography (PERG) at one and six months after injections. In addition, Optical Coherence Tomography (OCT) was used to show optic disc edema, which was followed by optic nerve head atrophy and marked thinning of the inner retina at 1 year. Histopathology of optic nerve cross sections showed decrements in optic nerve diameters of mND4-treated eyes and transmission electron microscopy showed significant loss of optic nerve axons in eyes injected with mutant ND4 (Yu et al., 2012).

1.9 WN1316 Compound

WN1316 is a novel small molecular compound, 2-[mesityl (methyl) amino]-N-[4-(pyridine-2-yl)-1H-imidazol- 2-yl] acetamide trihydrochloride, that was identified by performing *in silico* drug designing using a strategy called Anti-Oxidative Neuronal Cell Death- Quantitative Structure Activity Relationship (AOND-QSAR). In this strategy, the algorithm of the relationship between the chemical structure of the compound and its anti-oxidative stress activity is used. Several compounds were identified by this method that were

used as mother compounds for drug screening. Although these compounds possessed selective neuroprotection against oxidative stress-induced cell death and showed sustained motor function and slowed disease progression in ALS mice, their pharmacological weaknesses (including low water solubility and moderate toxicity) hindered their effective use. In further modification and optimization based on the chemical structure of different mother compounds, WN1316 was selected as a compound possessing high aqueous solubility, superior blood brain barrier permeability and low toxicity (Tanaka et al., 2014).

In vitro studies showed that WN1316 potently protected SH-SY5Y neuroblastoma cells against cell death induced by the oxidative stressors, menadione, α-naphthoquinone and 6-hydroxydopamine, although it was not protective against the non-oxidative stressors, staurosporine and okadaic acid. These studies also showed that WN1316 exerted its cytoprotective effects by elevating the expression of the NF-E2-related factor2 (Nrf2)-antioxidant response element-signalling pathway (Figure 3). Following treatment of SH-SY5Y cells with WN1316, Nrf2 was translocated to the nucleus where it induced transcription of anti-oxidant molecules such as HO-1 and NAD(P)H dehydrogenase [quinone] 1 (NQO1) (de Vries et al., 2008). WN1316 also exerts its cytoprotective effects by upregulating the Neuronal Apoptosis Inhibitory Protein (NAIP). NAIP was found to be up-regulated following WN1316 treatment of THP-1 cells in a dose dependent manner. It is thought that both Nrf2 and NAIP function independently in WN1316 cytoprotection (Figure 3) (Tanaka et al., 2014).

In vivo, WN1316 has shown potent cytoprotective effects against oxidative stress-induced cell death and neuronal inflammation in late-stage Amyotrophic Lateral Sclerosis (ALS) mice. WN1316 was able to preserve motor function, delay disease progression and

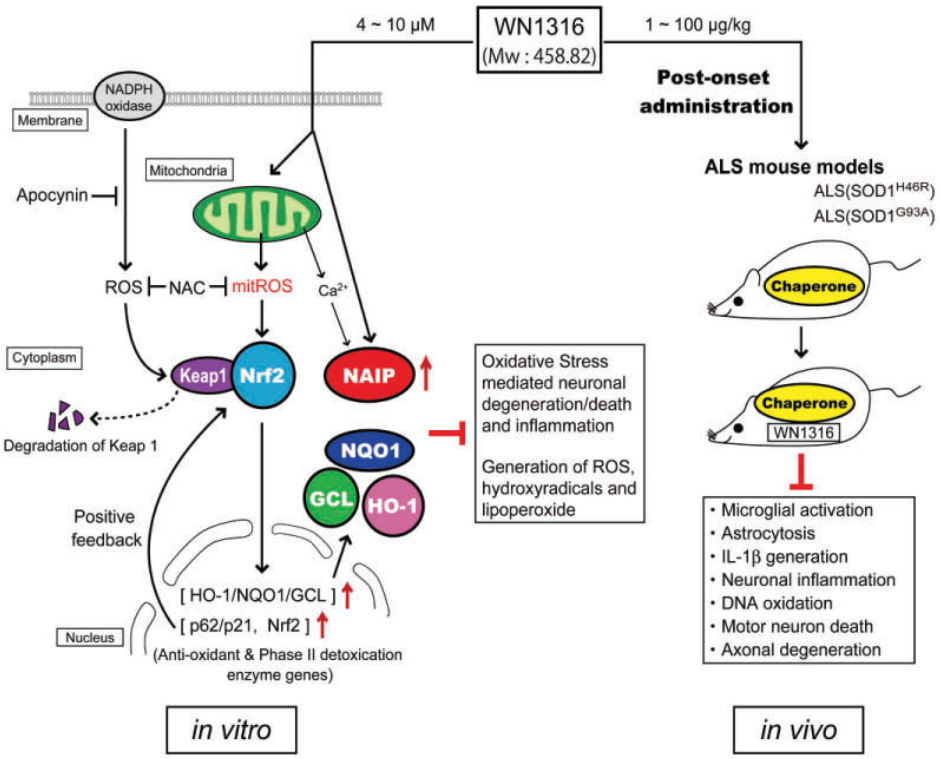

Figure 3.WN1316 mechanism of action. *In vitro*, WN1316 exerts its neuroprotective effects against oxidative stress-induced cell death via the up-regulation of endogenous NAIP and the activation of Nrf2 signaling cascade in an intracellular ROS-dependent manner which causes dissociation of Nrf-2 from the Nrf2-Keap1 complex and translocation of Nrf2 to the nucleus where it up-regulates anti-oxidant molecules. *In vivo*, post-onset administration of WN1316 to ALS mouse models causes suppression of glial activation and neuronal inflammation by inhibiting the generation of the inflammatory factor IL-1B, the reduction of oxidative damage, and the prevention of motor neuron death (Tanaka et al., 2014) .

prolong the post-onset survival interval of ALS mice. Additionally, WN1316 ameliorated motor neuron degeneration, inhibited axonal loss and caused suppression of the inflammatory factors interleukin-1 β (IL-1 β) and inducible nitric oxide synthase (iNOS) (Tanaka et al., 2014). WN1316 is ideal for therapeutic applications because it has high blood brain barrier permeability, very low toxicity and high water solubility. The LD50 in mice is approximately 20mg/kg body weight (J. Ikeda, pers. comm.), whereas the effective dose of WN1316 is 1-100μg/kg body weight/day in mice. Because of its excellent safety and efficacy profiles, WN1316 is currently in Phase I clinical trials for the treatment of ALS (https://upload.umin.ac.jp/cgi-open-bin/ctr_e/ctr_view.cgi?recptno=R000017516).

1.10 Hypothesis and Rationale for Thesis Research

Leber's Hereditary Optic Neuropathy (LHON) is a devastating retinal neurodegenerative disorder that leads to blindness in young adults and that is without cure to date. Mutations in mitochondrial genes that encode different subunits of Complex I of the Electron Transport Chain (ETC) result in oxidative stress (OS) that has a major role in LHON pathogenesis. WN1316 is a novel small molecule that was identified as a potent anti-oxidant and was shown to be effective in a mouse model of late stage Amyotrophic Lateral Sclerosis (ALS). WN1316 is currently in phase 1 clinical trials for the treatment of ALS. In the current study, we hypothesized that WN1316 will have therapeutic effects in the treatment of LHON because it specifically targets OS, which is the main pathway in disease pathology. *In vitro* and *in vivo* models of LHON were developed to test this hypothesis.

CHAPTER 2- MATERIALS & METHODS

2.1 *In Vivo* Studies

2.1.1 Animals:

Adult brown DBA/1J mice (n=50) at 8 weeks of age were purchased from Jackson Labs (Bar Harbor, Maine). Animals were maintained under standard laboratory conditions and used within two weeks of arrival. Procedures were performed in accordance with the ARVO statement for the Use of Animals in Ophthalmic and Vision Research and the guidelines of the University of Ottawa Animal Care and Veterinary Service.

2.1.2 Construction of the Recombinant Adeno-Associated Virus (AAV) Vectors:

AAV vectors encoding mutant ND4 or GFP (as a control) were obtained from William Hauswirth (University of Florida, Gainesville) with permission from John Guy (University of Miami, Florida). In brief, a cDNA construct, encoding the full-length, open-reading frame of the mutant version (11778G>A) of human ND4 with an ATPc mitochondrial targeting sequence appended to its N-terminus and the Flag epitope to its C-terminus, was inserted into a pTR vector. Expression was regulated by the CMV immediate early gene enhancer and under the control of the chicken β-actin promoter. A GFP construct was similarly generated for use as a surgical and viral control. Transgene expression was enhanced by inserting a woodchuck hepatitis post-transcriptional regulatory element (WPRE), which is used as a transcriptional enhancer in the 3'untranslated region of the construct. Recombinant AAVs of serotype 2 were packaged and purified. Details of viral constructs, viral purification and viral tittering can be found in Qi et al. (2007).

2.1.3 Intravitreal Injections:

Mice were sedated by inhalation with 2% isofluorane gas. Eyes were dilated using 1% tropicamide (Mydriacyl; Alcon Canada, Mississauga, ON, Canada). In fully dilated eyes, a local anaesthetic, proparacaine HCL (0.5%, Alcaine, Alcon) was applied topically to the cornea. To maintain corneal lubrication throughout the procedure, 0.3% hypromellose (Genteal gel; Novartis Pharmaceuticals Inc., Mississauga, ON, Canada) was applied to the eyes. Pain management was achieved by buprenorphine injections (0.04 mg/kg) directly before surgery.

Intravitreal injections were performed by creating a sclerotomy approximately 1-2 mm below the limbus with a 20-gauge V-lance knife (Alcon). Care was taken to avoid lens contact in order to prevent the development of a cataract. A 32-gauge blunt needle attached to a 10-µl syringe (Hamilton Company, Reno, NV, USA) was inserted through the scleral puncture and guided into the vitreal space. A volume of 1µl of $1x10^{12}$ viral genomes/mL (vg/mL) mND4 (AAV-mND4) or 1µl of $1x10^{12}$ vg/mL GFP (AAV-GFP) combined 50:1 with fluorescein tracer was delivered to the intravitreal cavity of the left eye and the right eye of each animal, respectively. The fluorescein allowed for immediate visualization and evaluation of the injection location, allowing ascertainment of a successful intravitreal delivery. Post-surgical care consisted of administration of the antibiotic B.N.P and buprenorphine (0.04 mg/kg) injection immediately after surgery. Buprenorphine (0.04 mg/kg) injection was also given one day after surgery.

2.1.4 WN1316 Treatment:

WN1316 (2-[mesityl (methyl) amino]-N-[4-(pyridine-2-yl)-1H-imidazol-2-yl]acetamide trihydrochloride) was provided by Dr. Joh-E Ikeda, synthesized by Wakunaga Pharmaceuticals Co., Ltd. (Japan). A stock solution of WN1316 (molecular weight: 458.82) was prepared by dissolving 1mg WN1316 in 1ml double distilled water. The stock was used for up to 2 weeks and was kept in a light-tight container at 4ºC and then made fresh again for the next set of treatments.

One week following the viral injections, animals were divided into 3 experimental groups. Group 1 received a daily dose of 100µg/kg WN1316 by oral gavage. At an average weight of 20g per animal, 2µl of the stock was diluted in an additional 200µl of distilled water to get a final concentration of 100µg/kg. Group 2 received an equal volume of water by oral gavage in order to control for the stress of the gavage procedure. Group 3 was the 'no gavage' control group. Treatment was repeated daily for 5 months.

2.1.5 Fundus Images and Electroretinography (ERG):

Retinal function testing (ERG) and fundus imaging were performed every two months. Retinal function was assessed using the Scotopic Threshold Response (STR) test. The STR was generated using the Espion system (Diagnosys LLC, Littleton). For the ERG, mice were weighed, then dark-adapted overnight and prepared for recording under red illumination. Under safe light conditions, animals were anaesthetized with intraperitoneal injections of a mixture of ketamine (100 mg/kg body weight) (Bimeda-MTC, Cambridge, ON) and medetomidine hydrochloride (1mg/kg body weight) (Domitor, Novartis, Finland). Pupils were dilated using 1% tropicamide (Mydriacyl; Alcon Canada, Mississauga, ON,

Canada). A local anaesthetic, proparacaine HCL (0.5%, Alcaine, Alcon Canada) was applied topically to the cornea. The animals were placed on heating pads to prevent loss of body temperature. Gold wire loop electrodes were placed on both corneas. Reference and ground electrodes were inserted in the mouth and tail, respectively. To prevent eye drying, and to ensure proper contact between the electrodes and the corneal surface, 0.3% hypromellose (Genteal gel; Novartis Pharmaceuticals Inc., Mississauga, ON, Canada) was applied to each eye before responses were recorded. The Ganzfeld apparatus was positioned over the animal's head. Single (blue color pulse) flash stimuli (4 ms duration) were presented at six increasing intensities ranging from $1x10^{-6}$ to 0.01 $Pcd.s/m^2$ using white color background of 6500K. Forty ERG traces were obtained and averaged for each luminance step. Response amplitudes were measured at fixed times after stimulus flashes representing the peak of the positive potential (110 ms after the flash) and at 200 ms corresponding to the trough of the negative potential in the dark-adapted ERG and plotted vs. stimulus energy. The analyses of ERG data presented in this thesis were conducted on all six steps. Fundus images were taken immediately after the STR using a Phoenix Micron III Retinal Imaging Microscope (Phoenix Research Laboratories, Inc).

Once all procedures were complete, the anaesthetic was reversed using 1mg/kg) of atipamezole hydrochloride (Antisedan, Novartis, Finland).

2.1.6 Tissue Fixation and Processing

Mice were euthanized using dry ice and were subsequently perfused transcardially with 5 ml phosphate-buffered saline (PBS) followed by 10 ml of Karnovsky's fixative (4% paraformaldehyde, 2% glutaraldehyde and 0.1 M sodium cacodylate in phosphate-buffered

saline, pH 7.4) in order to preserve tissue structure before dissection. The skull was opened up and the brain was carefully lifted off to expose the optic nerves. The optic nerves were cut at the optic disc on one end and below the optic chiasm on the other end and submerged in Karnovsky's fixative. Optic nerves were then embedded in resin prior to sectioning at 0.5µm and staining with 1% toluidine blue. Once the optic nerves had been sampled, the eyes were removed from perfused animals by cutting through the conjunctiva and extra-ocular muscles and releasing the eyeball. A small hole was made in the cornea using a needle to allow penetration of the fixative, and then eyes were placed in 4% PFA overnight. After fixation, eyes were washed for 3X with PBS and incubated in 30% sucrose overnight. This was followed by incubation in a 50:50 mixture of OCT- 30% sucrose for 1 hour, after which the eyes were oriented in small plastic trays filled with 50:50 OCT- sucrose and with corneas facing down. The trays were lowered onto a petri dish floating on liquid nitrogen for freezing. The frozen samples were stored at -80^{o} C until use. Samples were then sectioned at 10 microns in the saggital plane using a Shandon Electronic Cryotome (Thermo Scientific) at -20^{o} C. Six sections were obtained per slide. Sections were air dried for 2 hours, and stored at 4^{o}C to be used for histological analysis.

2.1.7 Analysis of Optic Nerve Cross-sections

Images of toluidine blue-stained semi-thin cross sections of 0.5µm from optic nerves were taken at 60x and 400x magnification under the MIRAX MIDI (Zeiss) microscope. Whole optic nerves cross sectional areas and diameters were calculated using Image J software. In addition, for each optic nerve, axon counts from six areas (a-f) were conducted using Image J software. For each of the 6 areas, a grid was overlaid and two squares (of 50x

20 μm) were chosen and axon counts were conducted within the squares. The mean number of axons per square was calculated, to give an average for each of the 6 areas, and then the 6 different areas were averaged to give a mean count for that particular optic nerve.

2.1.8 Optic Nerve Preparations for Transmission Electron Microscopy (TEM)

After fixation in Karnovsky's fixative, right and left optic nerves were cut under a stereomicroscope in the central region of the cranial portion of the nerve into a straight segment of 1mm of length. All segments were washed twice in 0.1M sodium cacodylate buffer for 1 hour and once for overnight. Segments were post-fixed with 1% osmium tetroxide for 1 hour and were washed in distilled water 2x for 5 min. Specimens were dehydrated in an ascending concentrations of alcohol and infiltrated in increasing concentrations of Spurr resin/acetone for 20 min, 6 hours and overnight. Segments were oriented inside molds and then polymerized overnight at 70^{o}C. Ultrathin sections (80nm) were collected onto 200-mesh copper grids and stained with 2% aqueous uranyl acetate and with Reynold's lead citrate. Sections were observed under a transmission electron microscope (Hitachi 7100) at 2000x, 4000x, 10,000x and 20,000x magnifications. Approximately 300 electron micrographs of the optic nerves were examined for their ultrastructural analysis. The individual who took the micrographs was blinded to the experimental groups.

2.1.9 Histological Analysis

Immunohistochemistry was performed on cryosections using Anti-RBPMS IgG (PhosphoSolutions) as a primary antibody, and Cy^3-conjugated AffiniPure Goat Anti-Rabbit

IgG (*Jackson ImmunoResearch*) as a secondary antibody. Slides were pre-fixed in 70% cold ethanol for 5 minutes, and blocked in 1% BSA in TBS with 5% goat serum for 20 minutes. Slides were then incubated in a humidified chamber at 4^{o} C with the primary antibody (1:500 in blocking solution with 0.3% Triton X-100, (Sigma)) overnight. The following day, slides were incubated for 1 hour with the secondary antibody (1:500) at room temperature. All washes were performed in TBS. Slides were counterstained with DAPI in the final washes, and mounted with Anti-fade and then cover-slipped. Stained sections were observed under fluorescence microscope (Zeiss Imager. M2, Zeiss Canada).

2.2 *In Vitro* Studies

2.2.1 Cell Culture

SH-SY5Y human neuroblastoma cells (purchased from ATCC) and 661W mouse photoreceptor-derived cells (kindly donated by MR Al-Ubaidi) were grown as sub-confluent monolayer cultures in DMEM/High Glucose medium (Hyclone) supplemented with antibiotics (penicillin 100U/ml; streptomycin 100µg/ml, Gibco), 10% Fetal Bovine Serum (FBS MULTICELL), 4mM L- Glutamine, 4500 mg/L Glucose and Sodium Pyruvate. Cells were grown in 10 cm tissue culture dishes and maintained in a humidified incubator at 37^{o} C in 5% CO2 with medium changed every 48 hours. Cells were split when they reached 70% confluency. They were washed twice with PBS, harvested by incubation in 2ml trypsin solution (Hyclone SH30042.01, Fisher Scientific) for 5 minutes, then were mixed with 4ml of medium and centrifuged at 3000G for 5 minutes, and cell pellets were suspended in fresh medium.

2.2.2 Anti-oxidative Stress-induced Neuronal Cell Death Analysis

2.2.2a Cell-Death Assay

Cells were transferred to 96-well plates and seeded at a density of 0.75 X 10^4 cells/well. When cells reached 60-70% confluency, they were pretreated with various concentrations of WN1316 compound dissolved in DMEM medium for 8 hours or vehicle (DMEM only) control. Cell death was induced by exposure to the oxidative stress triggers menadione (Sigma-Aldrich St Louis MO631003 USA) and H2O2 (216763-100ML, Sigma-Aldrich) at the indicated concentrations and for the indicated time points (see the results section).

2.2.2b Cellular Viability Using the AlamarBlue Assay

Following treatment with cytotoxins for 4 hours, cells were incubated overnight in complete medium containing 10% AlamarBlue solution (Invitrogen, DAL1100, Life Technologies). Optical density in each sample was measured using a plate reader (Biotek Synergy HT, Fisher Scientific). The intensity of the color developed in the medium is proportional to the viability of cells, which is calculated as the difference in absorbance between 570 and 600 nm (Scapagnini et al., 2004).

2.3 Statistical Analysis:

Analysis of data among the different groups was performed using two-way analysis of variance (2-way ANOVA). Values were expressed as the means ± SEM, and differences between groups were considered to be significant at *$p< 0.05$ and **$p<0.001$. Direct two-group comparisons were conducted using a 2-tailed student t-test.

CHAPTER 3- RESULTS

3.1 *In Vitro* studies

3.1.1 WN1316 Protects SH-SY5Y Neuronal Cells Against Oxidative Stress-Induced Cell Death by Menadione

WN1316 has previously been used as a therapeutic agent in the treatment of a mouse model of ALS (Tanaka et al., 2014). In that study, they examined the efficacy of WN1316 *in vitro* in the prevention of oxidative stress-induced cell death in the SH-SY5Y human neuroblastoma cell line. In order to test the efficacy of WN1316 in our hands, we conducted a preliminary experiment using the SH-SY5Y cell line to confirm that WN1316 replicates the previously obtained results. SH-SY5Y cells were cultured in growth medium and then treated with 10μM all-trans retinoic acid for 5 days to induce the differentiated neuronal phenotype. Differentiated cells (at approximately 70-80% confluency) were then pretreated with WN1316 for 8 hours and then incubated with menadione for 4 hours. The cytotoxin was then removed and cell viability was assessed using AlamarBlue (Figure 4). These studies showed that WN1316 does indeed prevent the death of SH-SY5Y cells treated with menadione. We found that 50μM menadione induced significant cell death in SH-SY5Y cells and that WN1316 was effective in protecting these cells. This protection was dose dependent with 10μM WN1316 giving the best outcome (Figure 4).

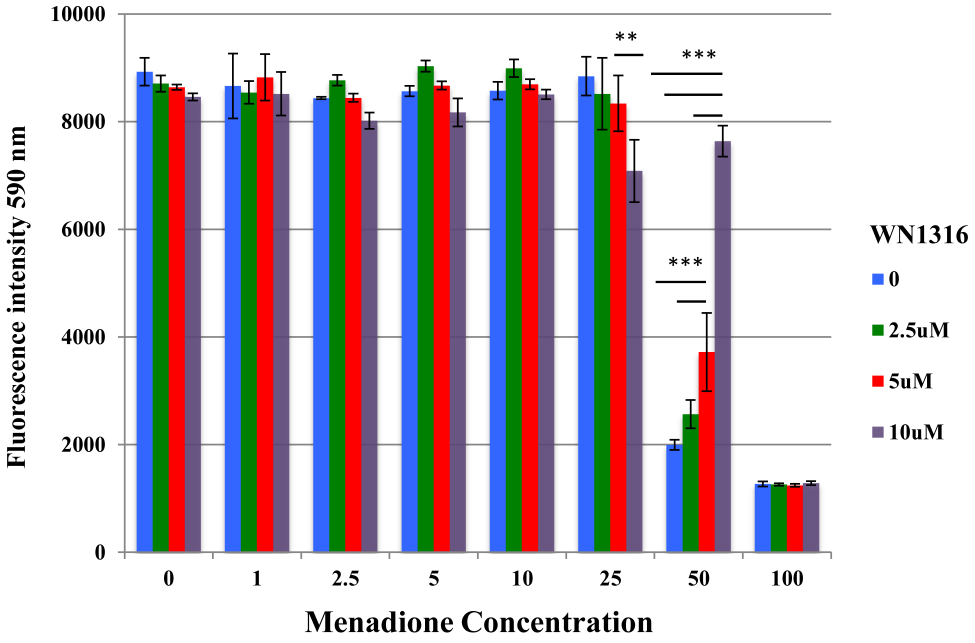

Figure 4. WN1316 protects SH-SY5Y cells against menadione-induced cell death. SH-SY5Ycells were pretreated with 2.5, 5 and 10µM WN1316 for 8 h at 37°C. The oxidative stress inducer, menadione, was added at concentrations ranging from 1-100 µM and incubated for 4 h. Cell viability was measured using the AlamarBlue assay by measuring optical density using a plate reader, where the intensity of the color developed is proportional to the viability of cells. Menadione at concentrations between 1-25 µM did not cause decrease in cell number. Cell death occurred only at concentrations of menadione higher than 25µM. Significant cytoprotection against 50µM menadione was achieved with concentrations of WN1316 above 2.5µM. This effect was dose-dependent and 10µM WN1316 gave the best neuroprotection. Data are expressed as mean ±SEM. **p<0.001, ***p<0.0001 by two-way ANOVA.

3.1.2 WN1316 Protects 661W Cells Against Oxidative Stress-Induced Cell Death

3.1.2a) WN1316 protection in the Menadione Assay

The defect associated with LHON is found in retinal ganglion cells. Since there are no available retinal ganglion cell lines, and it is difficult to prepare primary retinal ganglion cells due to their limited capacity for cell division, we used 661W cells to assess the effects of WN1316. 661W cells are a mouse cone photoreceptor-derived cell line immortalized by the expression of simian virus (SV) 40T-antigen. These cells exhibit neuronal cell characteristics and express photoreceptor markers such as opsin, transducin and arrestin (Tan et al., 2004). Although photoreceptors are post-mitotic and 661W cells are rapidly dividing, these cells are used extensively in the literature as a surrogate for the retina in culture and they can offer insights into therapeutic effects on photoreceptors.

The ability of WN1316 to protect 661W cells against the oxidative stress-induced cell death by menadione and hydrogen peroxide was tested. First, a cell death assay was performed to determine the ideal conditions for the assays. In the case of menadione, a range of concentrations was tried to induce 661W cell death. Figure 5A shows a 90% decrease in viable cell number occurring between 10 and 25μM menadione. Therefore, another experiment was performed using different concentrations between 10 and 25μM to determine the exact concentration of menadione for the subsequent assays. This showed a steady decline in cell viability from 12.5μM to 20μM menadione (Figure 5B). In the next experiment, the protective effects of WN1316 were investigated against these concentrations of menadione. Both concentrations of WN1316 (3 and 5 μM) were significantly protective against all concentrations of menadione, and this effect was dose dependent (Figure 6). WN1316 was safe and did not cause cellular toxicity at the concentrations tested.

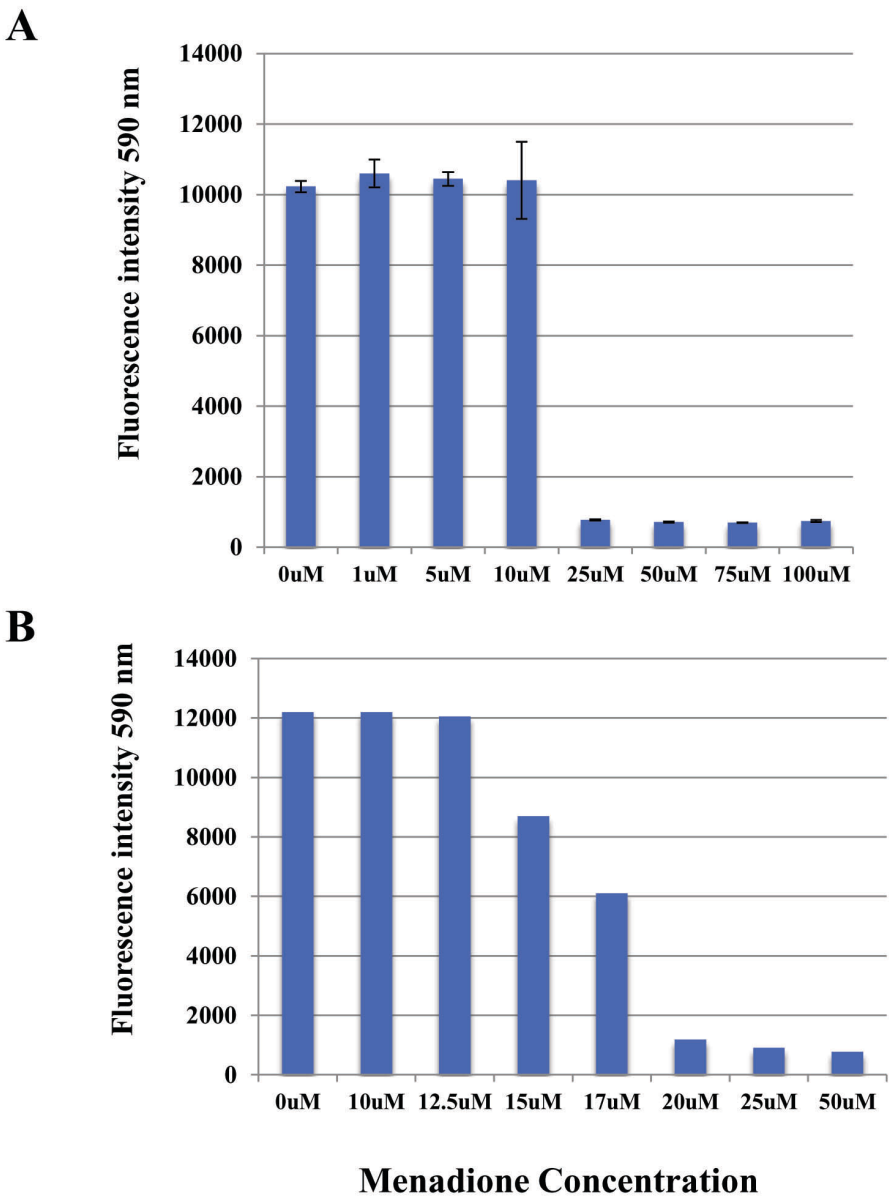

Figure 5. Menadione Cell Death Assay in 661W cells. Cell death was induced using the oxidative stressor menadione. A) To determine the effective concentrations of menadione, a cell death assay was performed, finding that potent cell death is occurring between 10 µM and 25 µM of menadione. **B)** Different concentrations between 10 and 25µM were used to determine the exact effective concentration of menadione that showed a steady decline in cell viability from 12.5µM to 20µM menadione. Data are expressed as mean ±SEM.

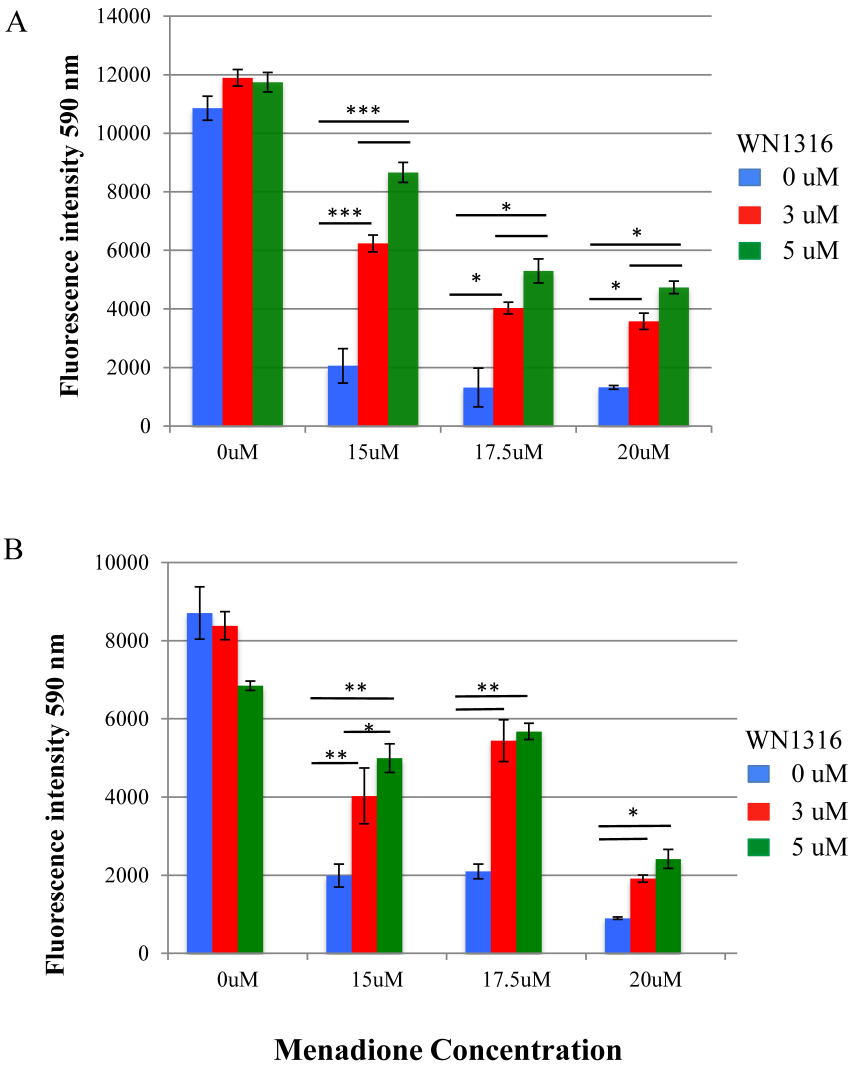

Figure 6. WN1316 protects 661W cells against menadione-induced cell death. In two separate experiments (A and B), 661W cells were pretreated with 3 or 5 µM WN1316 for 8 h at 37°C. The indicated doses of menadione were added and incubated for another 4 h. The cell viability was measured by AlamarBlue assay. The protective effect of WN1316 is dose-dependent. Data are expressed as mean ±SEM. WN1316 significantly protected 661W cells at all concentrations (2-way ANOVA, *p<0.05, **p<0.001, ***p<0.0001).

3.1.2b) WN1316 Effects in the Hydrogen Peroxide (H_2O_2) Assay

The protective effects of WN1316 on 661W cells were tested in a second oxidative stress-inducing compound, H_2O_2. A preliminary death assay was conducted in 661W cells to determine the optimal doses of WN1316 and H_2O_2. We found that an 8-hour treatment with H_2O_2 was toxic to all the cells (data not shown), so subsequent treatments were only conducted for 4 hours. In addition, we noticed that 6 μM of WN1316 compound alone was toxic to cells, and while 3μM was not toxic, it was also not protective against hydrogen peroxide induced cell death (Figure 7).

In order to determine the optimal conditions for future H_2O_2 experiments, a kill curve was conducted with different concentrations of H_2O_2 over longer periods of treatment times. These studies were highly variable, but suggested that a concentration of 1mM was inducing significant cell death in 661W cells (Figure 8). Consequently, several concentrations, up to and including 1mM were tested in a neuroprotection study with WN1316. The results of this study were highly variable (Figure 9A); therefore, I used higher concentrations at 1.5 and 2mM, which caused 66% and 84% cell death, respectively (Figure 9B). Importantly, WN1316 at 3 and 5 μM significantly suppressed cell death and increased cell viability (Figure 9B).

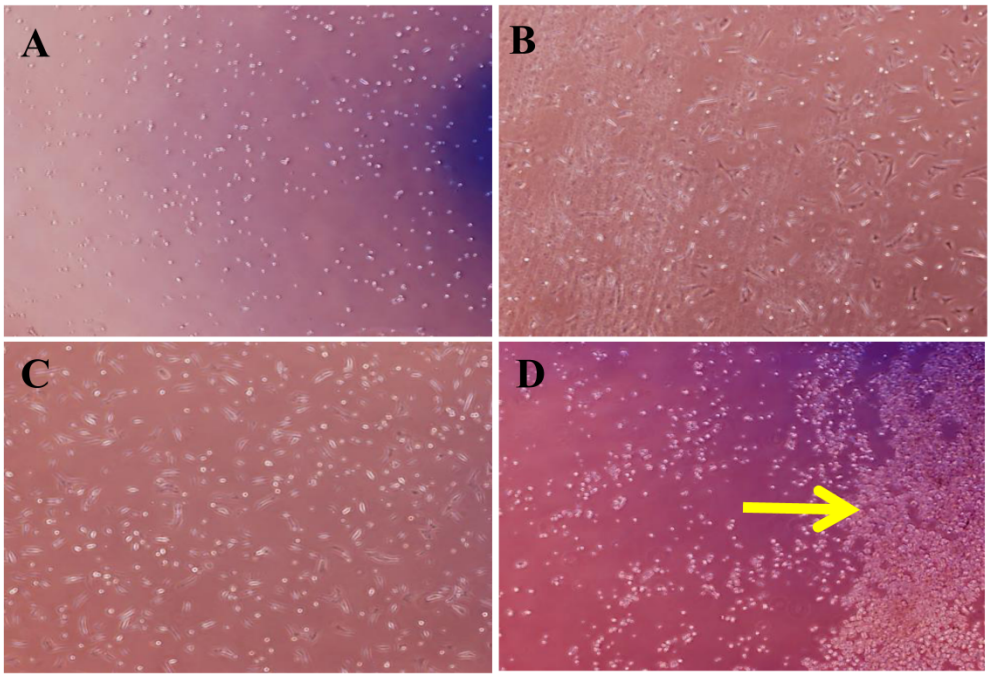

Figure 7. The effects of WN1316 treatment on 661W cells. Cells were pretreated with 3 and 6 μM WN1316 for 8 h followed by treatment with 500 μM H2O2 for 4 h. A) 6μM WN1316 alone is toxic to 661W cells. Cells are rounded and have started to lift off the plate . B) The vehicle, DMSO shows no toxicity in 661W cells (cells are adhered to the plate and have a rod-like appearance). C) 661W cells treated with 3μM WN1316 exhibit no toxic effects (they are similar to the cells in B). D) 661W cells treated with 500 μM H2O2 are not protected by 3μM WN1316, as is shown by all the floating dead cells in the culture (yellow arrow identifies cells that have similar rounded morphology to the cells in A, and have lifted off the plate).

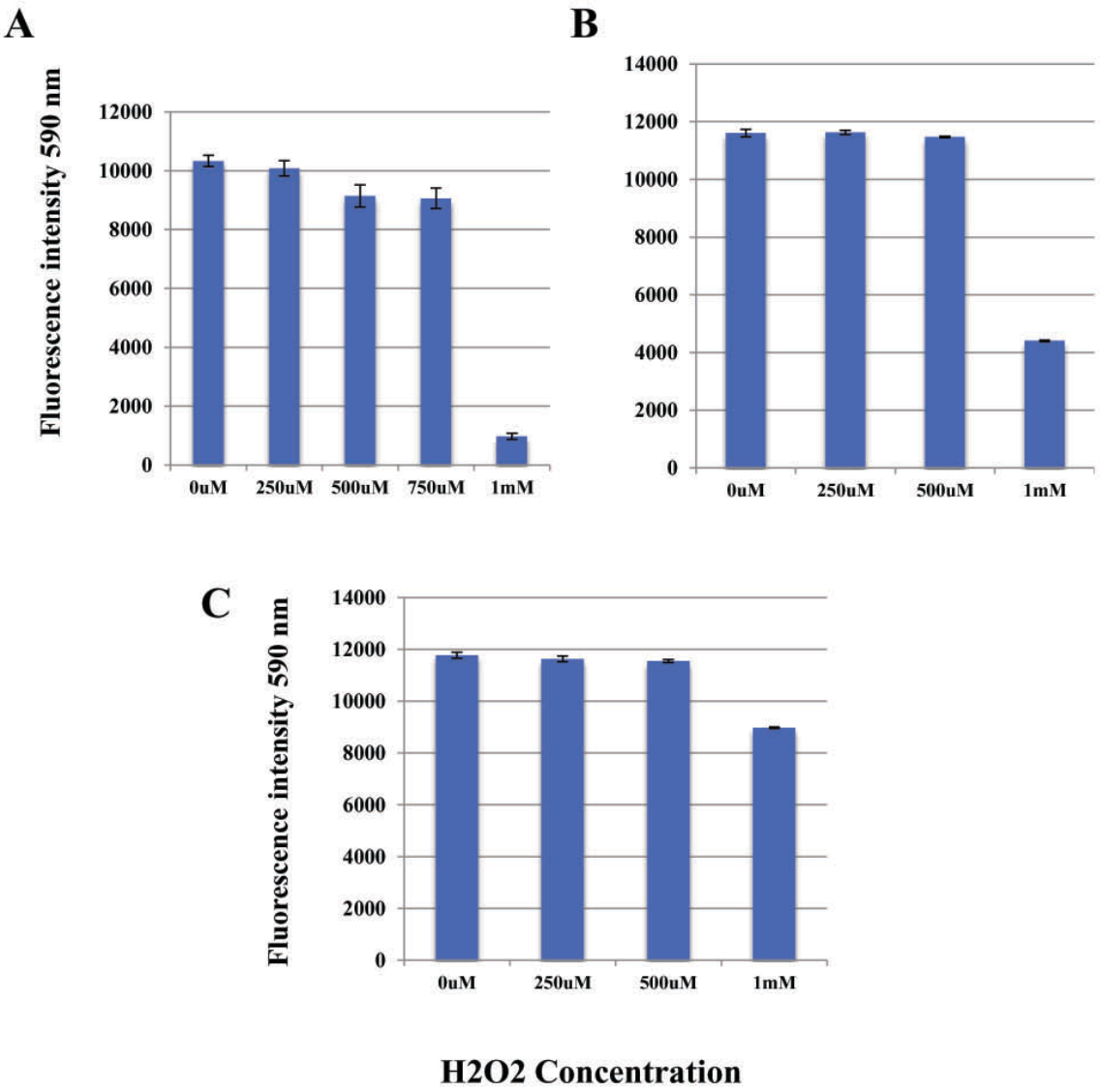

Figure 8. H2O2 death assay in 661W cells. 661W cells were treated with the indicated doses of H2O2 to determine the most effective concentration. A) Effects of 4 h treatment of H2O2 on 661W cell viability. B) Effects of 6 h treatment with H2O2 on 661W cell viability. C) Effects of 24 h treatment with H2O2 on 661W cell viability. H2O2-induced cell death was highly variable in the assays. Data are expressed as mean ±SEM.

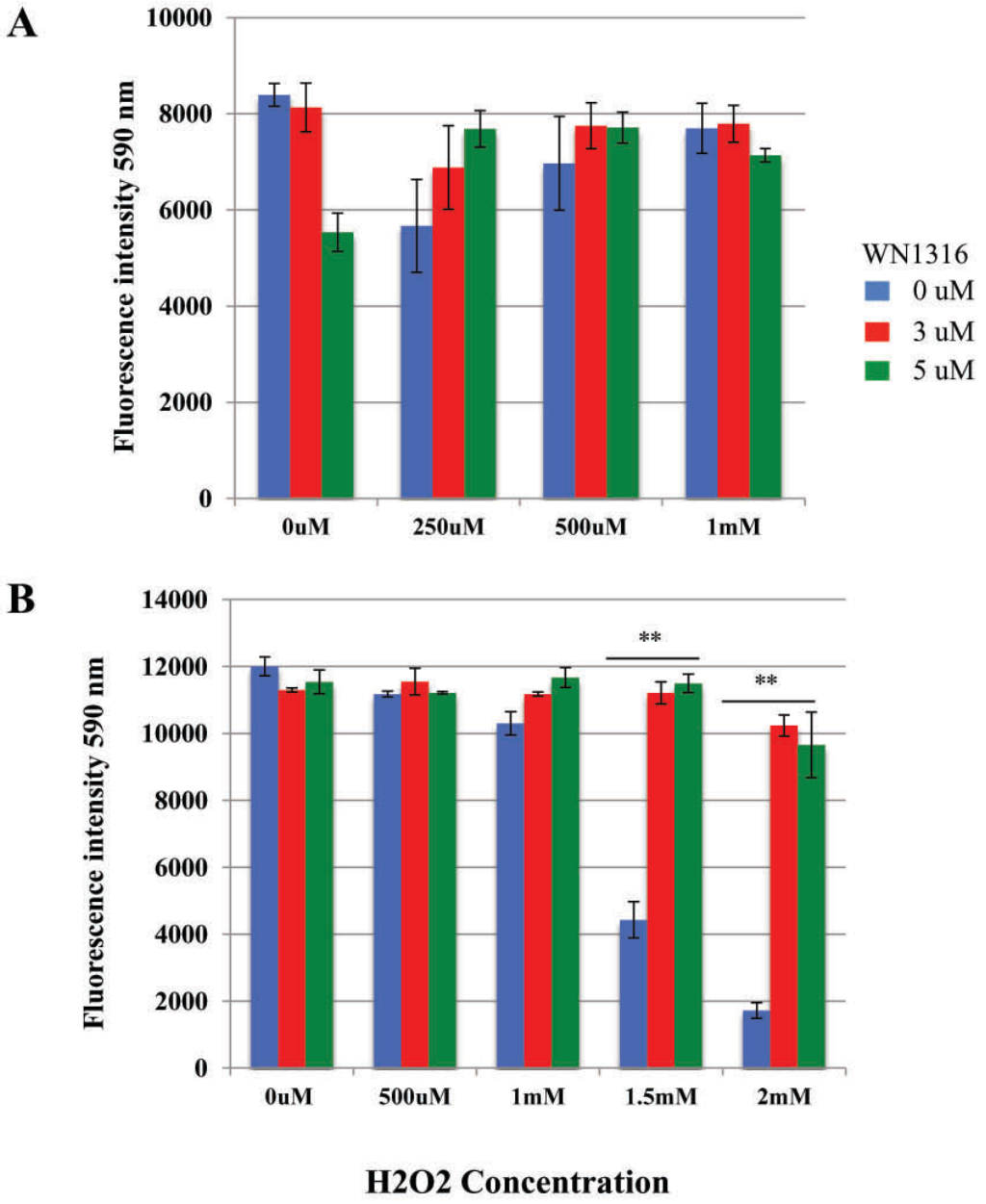

Figure 9. WN1316 protects 661W cells against H2O2-induced cell death. 661W cells were pretreated with WN1316 for 8 h prior to the exposure to H2O2. A) In contrast to the results obtained in Figure 6, 1mM H2O2 did not cause significant cell death in this assay. Therefore, increased concentrations were used in B). Results in B) show increased survival in response to WN1316 treatment. This effect is seen at both doses of WN1316. Data are expressed as mean ± SEM. ($^{**}P<0.001$) by two-way ANOVA.

3.1.3 Combination Therapy with WN1316 and X-linked Inhibitor of Apoptosis (XIAP)

Many retinal diseases (including LHON) have both oxidative stress and apoptosis involved in disease pathology. Therefore, we decided to test a combination therapy targeting both of these processes. We targeted apoptosis using XIAP and oxidative stress using WN1316. For these studies, I used 661W cells that had been generated by another graduate student in the lab (Sarah Wassmer) that stably over-expressed either XIAP (referred to as 2088 cells) or the pCI empty plasmid vector. Cells were maintained under G418 selection and transferred to G418-free media 24 hours prior to their use in the death assays. When cells reached 60-70% confluency, they were pre-treated with WN1316 for 8 hours prior to 4 hours treatment with the toxic agent.

In comparison with 661W cells, cells stably transfected with XIAP show a significant increase in survival rate. Following treatment with menadione (15μM) survival rate in 661W cells is 20% compared with 50% in 2088 cells (compare blue bars in Figures 10A and B, ($p<0.005$)). The addition of WN1316 further increased this survival: in 661W cells 3μM WN1316+15μM menadione resulted in 45% survival while in 2088 cells, the same doses resulted in 78% survival (see red bars in 10). 661W-pCI cells were more susceptible to cell death than 661W cells alone (compare Figure 6 and 10). This may be due to the fact that 661W-pCI cells were under selection with G418, and G418 can be stressful on cells. Consequently, it is expected that the combination of XIAP and WN1316 (in 2088 cells) seen in Figure 10 is also an underrepresentation of the survival effect, since these cells were also under selection. In the case of H2O2; as seen previously with 661W cells alone, 1mM H2O2 resulted in great deal of variability in 2088 and pCI cells which made it difficult to assess neuroprotective effects of WN1316 (Figure 11).

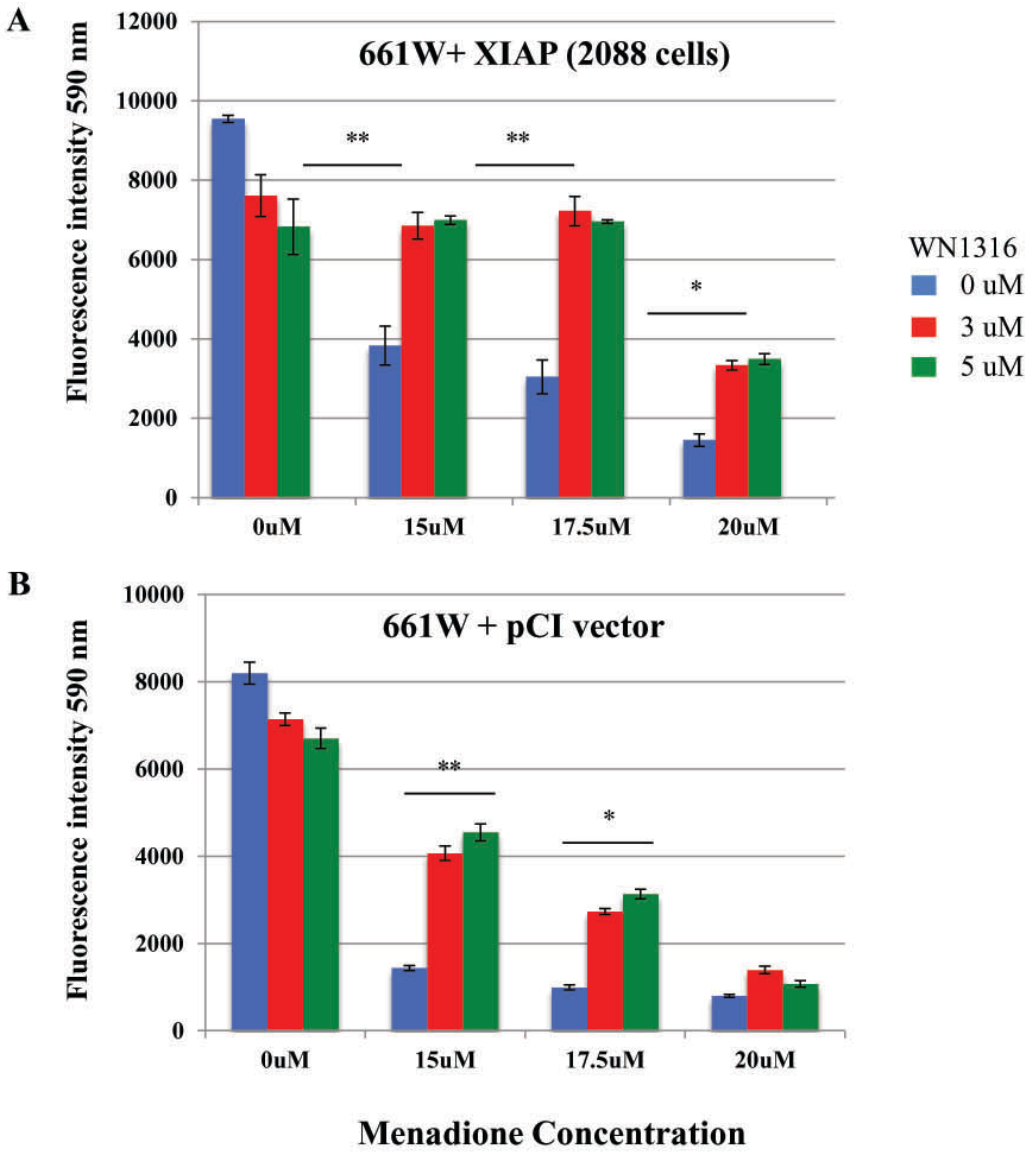

Figure 10. Combination therapy of XIAP and WN1316 has the best survival outcome following menadione treatment. A) 2088 cells (661W cells stably transfected with XIAP) show increased survival following menadione treatment (compare blue bars in A and B). The addition of WN1316 further improves this survival. B) In pCI-transfected 661W cells (661W cells with empty vector as a control for XIAP transfection), menadione caused a greater decline in viable cell number as compared to 661W cells alone (see Figure 6); this effect is likely due to the fact that the cells are under selection with G418. Data are expressed as mean ±SEM. ($^{*}P<0.05$) ($^{**}P<0.001$) by two-way ANOVA.

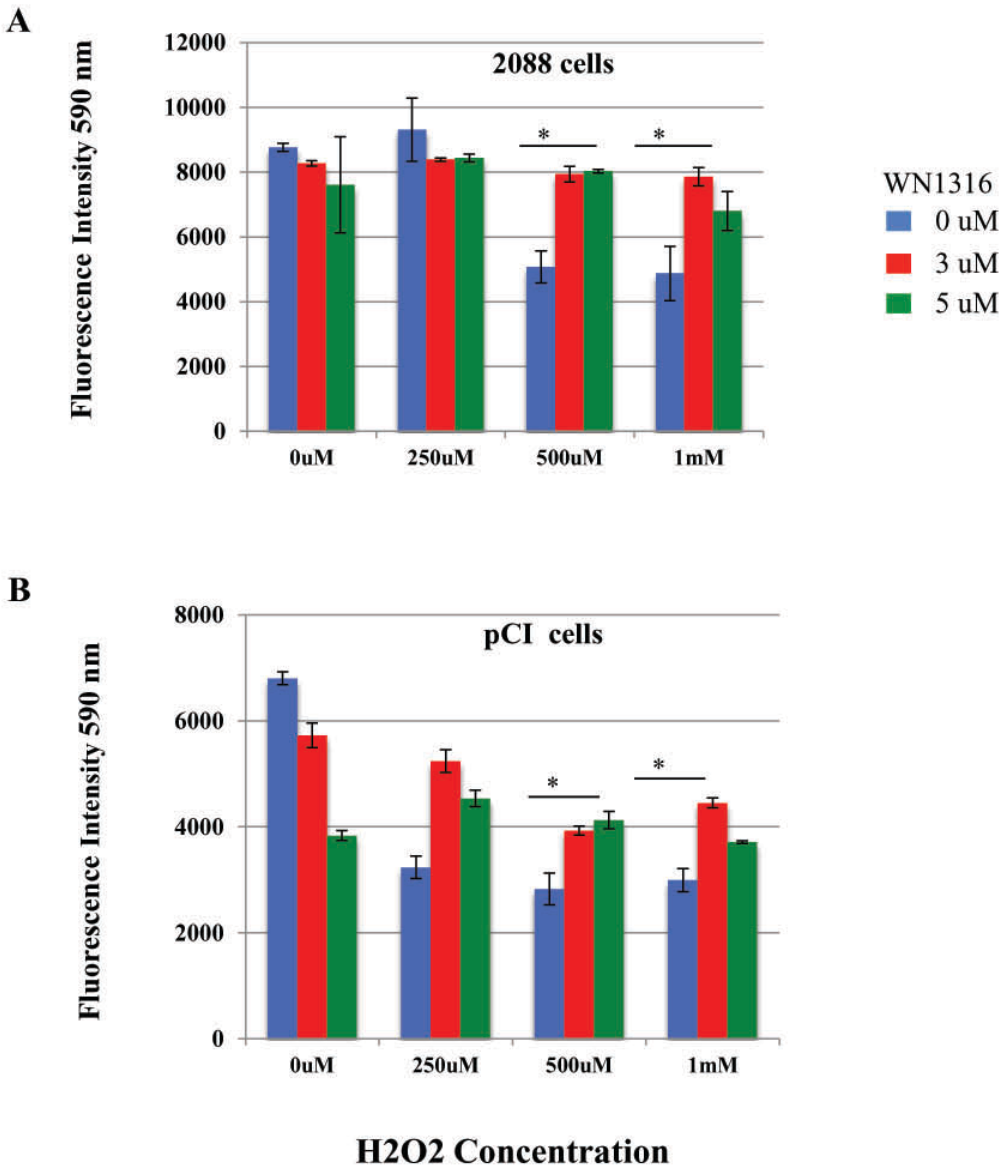

Figure 11. Combination therapy with XIAP and WN1316 following H2O2 treatment is not as conclusive as menadione treatment due to variability in the H2O2 effect. In all cases, cells were pre-treated with WN1316 for 8 h prior to exposure to H2O2 overnight. AlamarBlue assay was used to assess cell survival. There is considerable variability in the effect of H2O2. H2O2 caused cell death in A) 2088 cells and B) pCI cells only at higher concentrations, and WN1316 showed a significant protective effect. Data are expressed as mean ±SEM. ($^{*}P<0.05$) by two-way ANOVA.

3.1.4 Toxicity of WN1316

To evaluate the safety of WN1316, we tested different concentrations of the compound (3,5 and 7μM) to assess its toxicity in 2088 cells. As with previous studies in 661W cells, WN1316 was toxic at high concentrations (7μM). Moreover, this effect appeared to be worsened by the presence of G418 (Figure 12).

3.2 In Vivo Studies

We generated an LHON model in the DBA/IJ strain of mice by intravitreally injecting a mutated form of the NADH ubiquinone oxidoreductase subunit 4 (mND4) gene that was packaged in an adeno-associated virus, and targeted to RGC mitochondria by fusing a mitochondrial targeting sequence (MTS) to the N-terminal end of the mutant gene. Animals received an injection of 1μl of $1x10^{12}$ mutant ND4 viral particles/ml in one eye and 1μl of $1x10^{12}$ GFP viral particles/ml in the contralateral eye. One week after injections, animals were divided into 3 groups: Group1 received a daily dose of 100μg/kg of animal weight of WN1316 dissolved in 200μl of distilled water by oral gavage; Group 2 received a daily dose of the same volume of distilled water, and Group 3 was the control group (no gavage).

Since Pattern Electroretinography (PERG) had been used in the literature to assess retinal ganglion function, we conducted baseline PERGs in all animals so that we could later assess the effect of the disease on RGC function. However, with our ERG system, PERGs were highly variable and noisy in all animals, so we decided to assess retinal function using the Scotopic Threshold Response (STR) test. Fundus images were taken immediately after the STR (every two months) to monitor retinal health and to assess expression from the virus (Figure 13). At the end point of the experiment, eyes and optic nerves were sampled and

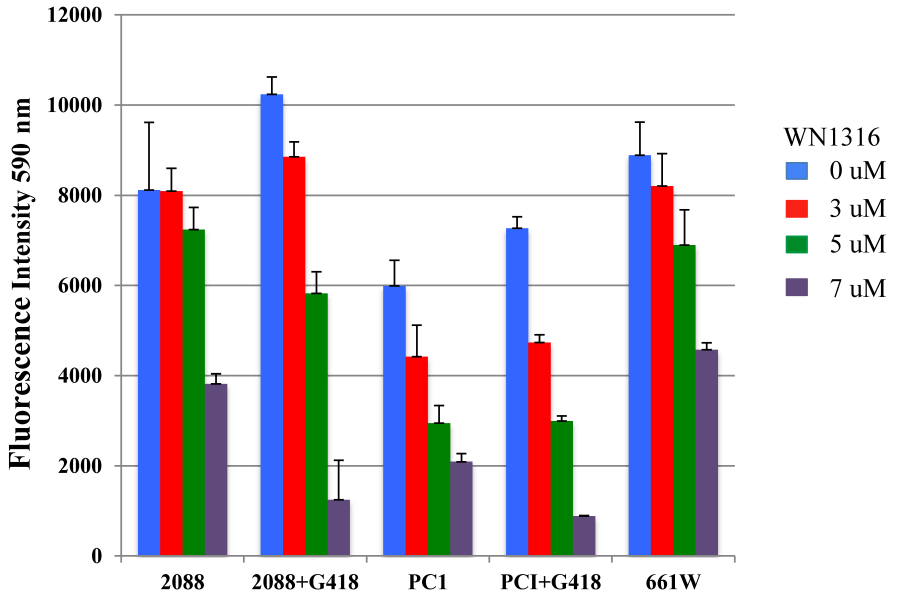

Figure 12. WN1316 is toxic to 661W cells at higher concentrations and this effect is exacerbated by the selection with G418. 661W cells over-expressing XIAP (2088) and pCI vector control cells were maintained under G418 selection. Prior to this experiment, cells were transferred to media without G418. When cells reached 60% confluency, they were treated with WN1316 for 8 h. Cell viability was then assessed by incubation with 10% AlamarBlue overnight.

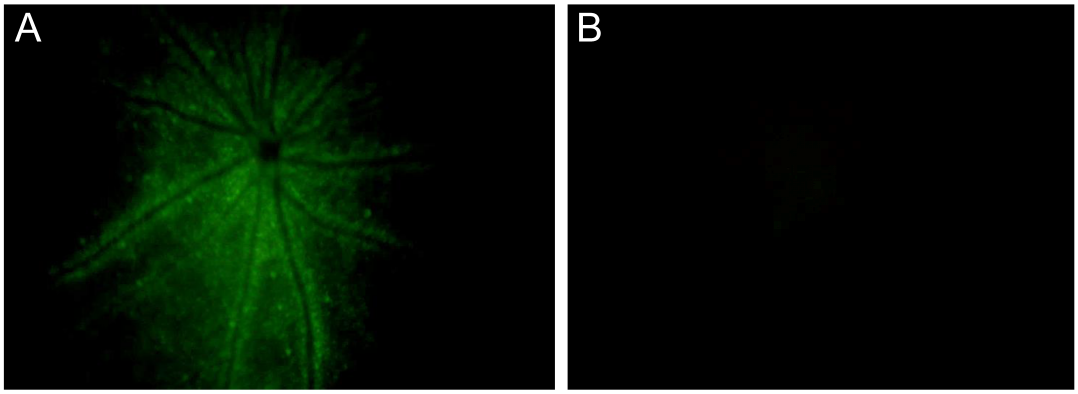

Figure 13. AAV virus is expressed in RGCs. A) Live fundus images, taken 4 months following intravitreal injection of AAV virus, show good expression of the GFP protein and good coverage by the virus in the RGC layer. B) Contralateral non-GFP injected eye shows no fluorescence

sectioned. The eyes were used for immunohistochemical analysis, and the optic nerves were stained with toluidine blue for measurements of cross sectional areas and diameters, axon counting, or used for electron microscopy (EM) analysis to assess optic nerve integrity.

3.2.1 WN1316 effects on the STR ERG at 4 months

Four months following the viral injections of mND4, disease progression was not evident by ERG analysis. Comparison of mND4 versus GFP-injected eyes did not show any differences in the ERG, regardless of the experimental group (WN1316, water gavage or no gavage) (Figure 14). Interestingly, however, the ERGs in the WN1316 animals (irrespective of whether they had been injected with mND4 or GFP) is higher than in the other groups (17% and 25% increase in GFP-and mND4 injected eyes respectively) although this trend did not reach significance. In addition, the ERGs in the WN1316 group were very similar or even better than non-injected, normal control animals (Figure 14). This trend was seen in all 6 steps of the STR test. The literature suggests that loss of RGCs occurs with advancing age (Neufeld & Gachie, 2003). This may suggest that WN1316 is protecting RGCs from age-related normal degeneration, but additional axon counts need to be conducted to determine if this is the case.

3.2.2 Optic nerve measurements show no evidence of disease progression

Image J software was used to perform optic nerve measurements of cross-sectional areas and diameters in toluidine blue-stained sections (Figure15). Diameters and areas were tested because we reasoned that thinning of the optic nerve might suggest that the disease process was underway. However, this analysis did not show any differences in optic nerve measurements between mND4 and GFP-injected eyes (Figure 15).

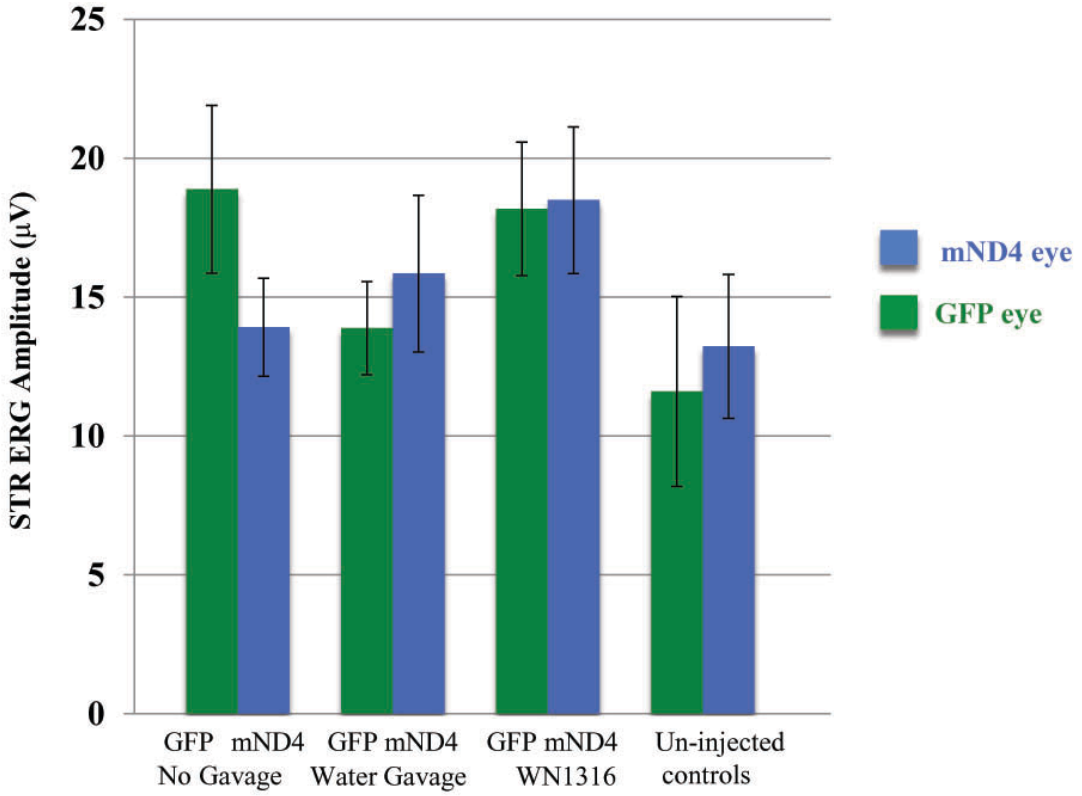

Figure 14. WN1316 appears to improve the STR ERG (although the effect is not significant). The ERG protocol involved 6 steps of increasing intensity of light. The STR is maximal in step 4 (shown above). A similar trend, with WN1316-treated animals showing a slightly improved ERG, was seen in all the steps (1-3, 5-6) as well. N=24 for WN1316 group. N=13 for water gavage group, N=11 for no gavage group. Data are expressed as mean ±SEM.

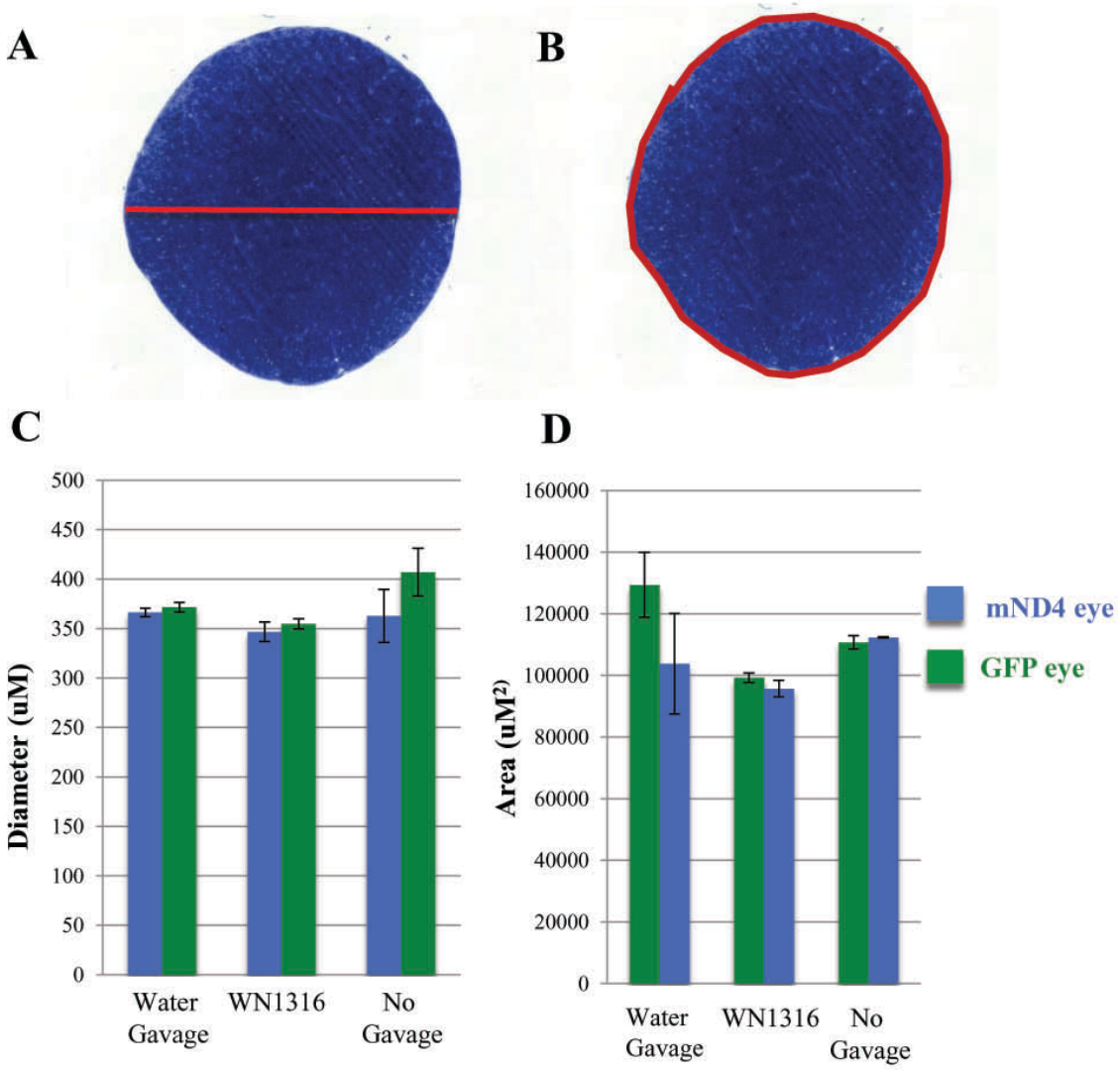

Figure 15. Optic nerve measurements do not show disease progression. For each optic nerve, Image J was used to measure the diameter (A, C) and whole cross sectional area (B, D). Optic nerve measurements show no evidence of disease progression. Measurements of the optic nerve diameter (C) and area (D) comparing the different groups showed no significant effects of the disease or the compound. Measurements were taken at the same distance from the optic cup for each animal. For WN1316, N=5 (5 eyes for GFP and 5 eyes for mND4). For each of the other groups, N=2 (2 eyes for GFP and 2 eyes for mND4). Data are expressed as mean ±SEM.

3.2.3 Number of axons is not significantly changed by WN1316 treatment

Image J software was also used to conduct axon counts in mND4 and GFP-injected optic nerves for each of the treatment groups (WN1316, water gavage and no gavage). For this analysis, 6 different images were taken in each optic nerve, and two separate areas were counted for each of the 6 images. All the numbers were averaged to obtain a mean axon count per optic nerve. This analysis also failed to show a difference between mND4 and GFP-injected eyes, further reinforcing that the disease had not progressed sufficiently to cause loss of retinal ganglion cells (Figure 16).

3.2.4 Immunohistochemistry was inconclusive

In order to assess the effects of WN1316 therapy on retinal ganglion cell structure, eyes were cryo-embedded, sectioned, and stained with the RGC-specific antibody, RNA-binding protein with multiple splicing (Rbpms). Interestingly, Rbpms staining was specific and clear in the control samples, but only provided background fluorescence in multiple samples treated with WN1316 (Figure 17). This made it difficult to do RGC counting in the different treatment groups. The reason for the lack of specific Rbpms binding in the WN1316 group is difficult to explain, especially since specific Rbpms binding was found in water gavage and control (no gavage) animals. It is possible that WN1316 treatment somehow interferes with the binding of the antibody or that the WN1316 may have somehow altered the fixation and processing conditions of the tissues to prevent antibody binding. Nevertheless, it is doubtful that Rbpms staining would have revealed differences in RGC counts since the axon counts did not show sufficient disease progression to result in RGC loss.

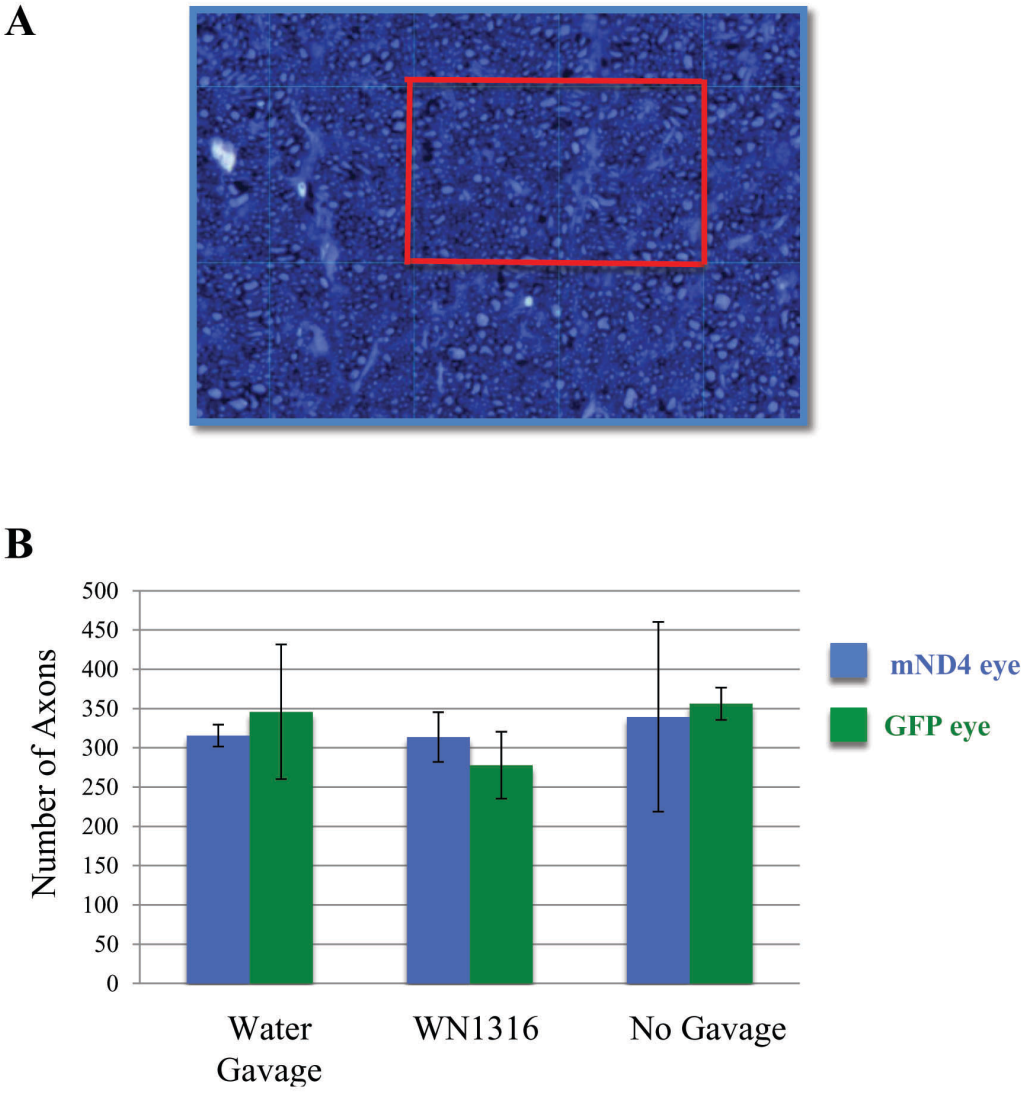

Figure 16. Axon counts do not show disease progression. A) For each animal, a grid (20X50 uM) was used to ensure that the same cross-sectional area was counted (12 squares were counted from six areas and then averaged for each optic nerve). B) A barplot shows axon counts from optic nerves from three different treatment groups stained with toluidine blue (n=6 for WN1316 group, n=4 for each of the Water and No Gavage groups). No significant difference in the number of axons between the groups is demonstrated. Data are expressed as mean ±SEM.

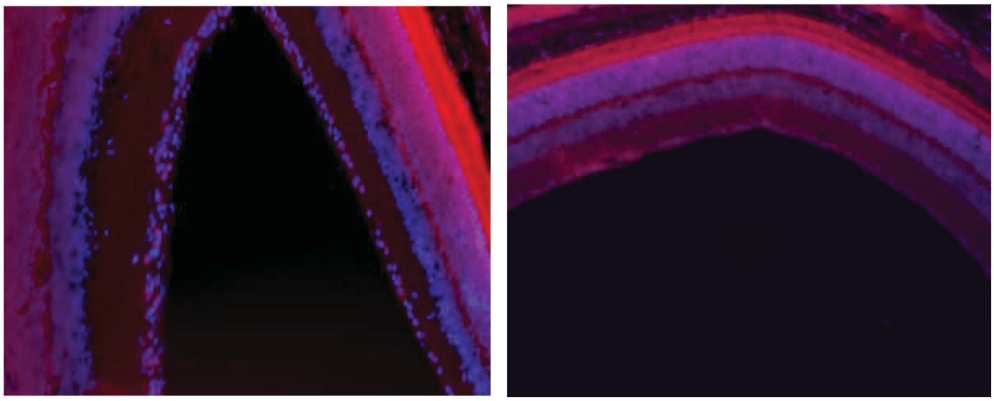

WN1316-treated- LE WN1316 treated -RE

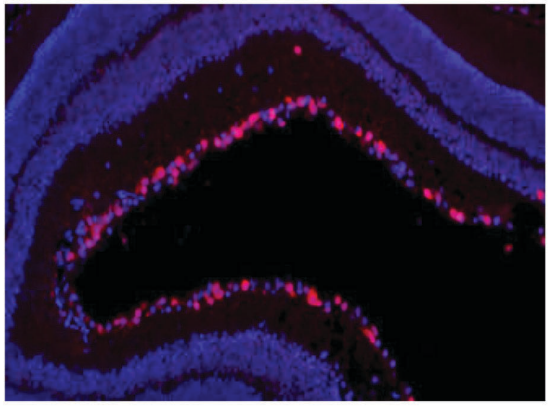

No gavage-RE

Figure 17. Histology with Rbpms antibody. Histological analysis of the cryosections stained with the RGC-specific antibody Rbpms revealed that there is no specific binding to the antibody occurring only in the sections taken from WN1316 treated tissues . Sections from the no-treatment groups are showing specific binding. This made it difficult to do RGC counting in the different treatment groups. LE – left eye, RE – right eye.

3.2.5 Electron Microscopy shows that mND4 causes LHON

Although the ERG was not affected by disease progression, and the analysis of histological sections was inconclusive, Electron Microscopy (EM) analysis of the optic nerves gave indications of the disease, showing signs of advanced nuclear fragmentation, apoptotic cell bodies and lots of white processes (Figure 18). The EM analysis was conducted by Yves de Repentigny (Rashmi Kothary lab, OHRI), who was blinded to the experimental groups and was, nevertheless, able to identify the mutant ND4-injected eyes based on the images.

3.2.6 Water gavage has no effect

As shown in Figure 19, water gavage treatment has no effect on disease progression nor does it have a therapeutic outcome. In the GFP injected eye, optic nerve axons are healthy, and the nucleus and cytoplasm have a normal healthy appearance. However, in the mutant ND4-injected eye treated with water gavage, optic nerves continue to lose myelination (white circular bodies in B1) and black apoptotic bodies and white processes are indicating that glial cells are degenerating.

3.2.7 WN1316 appears to slow disease progression

In the mND4-injected eyes that received the WN1316 treatment, EM images showed slower nuclear fragmentation compared to the animals that received water gavage or no treatment (Figure 20). Moreover, there was a delay in disease progression shown as decreased apoptosis, and more preservation of cellular components only in the WN1316 group (Figure 20) in comparison to the no-treatment group where cells are undergoing cell death. This analysis was conducted on a small number of animals, making quantification

difficult. As expected, the GFP-injected eye treated with WN1316 has normal processes indicating normal glial cells with normal healthy nuclei.

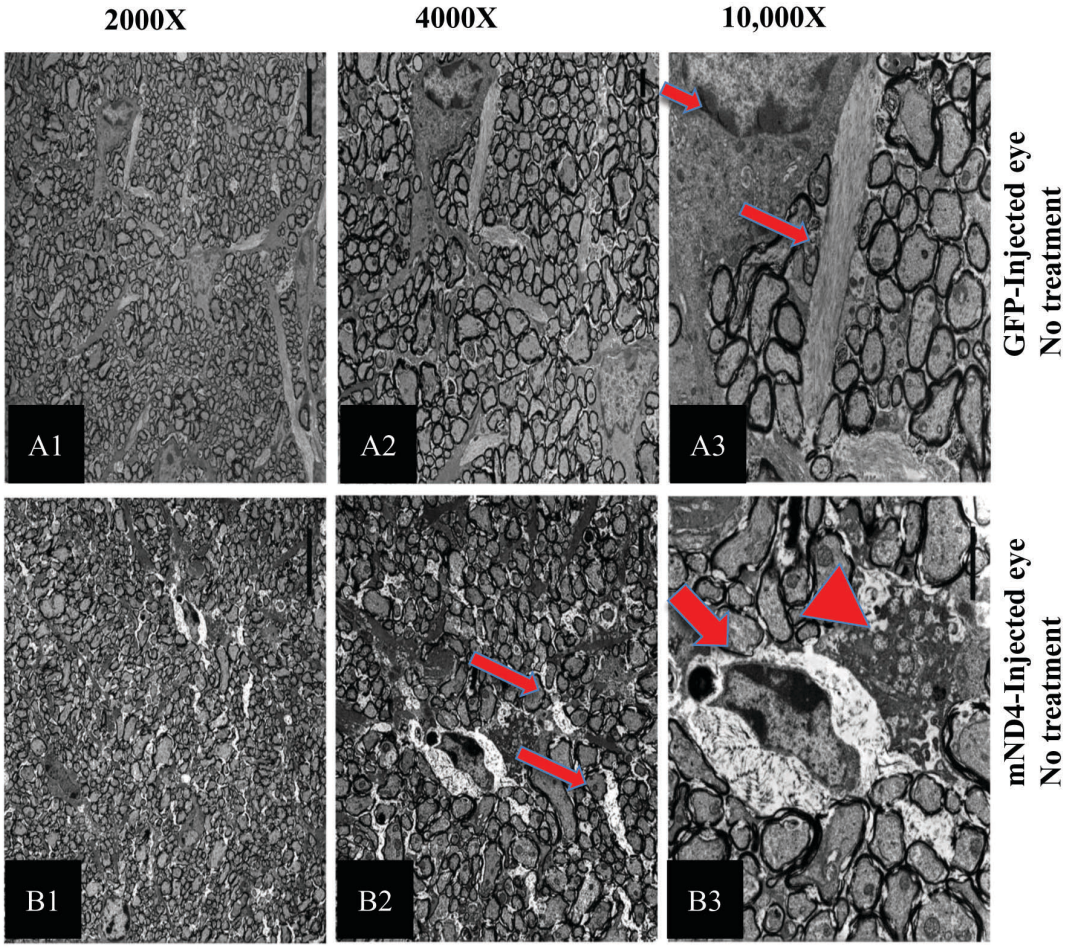

Figure 18. mND4 causes LHON. A1-A3 show an optic nerve from a GFP-injected animal, and B1-B3 are cross-sections of an optic nerve from a mND4 injected animal in the no-treatment group. The white processes in B2 (arrows) are indicating a decrease in myelination, implying that oligodendrocytes are affected. B3 (mND4 injected eye) is showing an apoptotic cell body and nuclear fragmentation (arrow) and an adjacent dying cell with condensing cytoplasm (arrow head). In A1-A3 (GFP injected eye), there are normal processes implying healthy oligodendrocytes and the cell cytoplasm is in good condition.

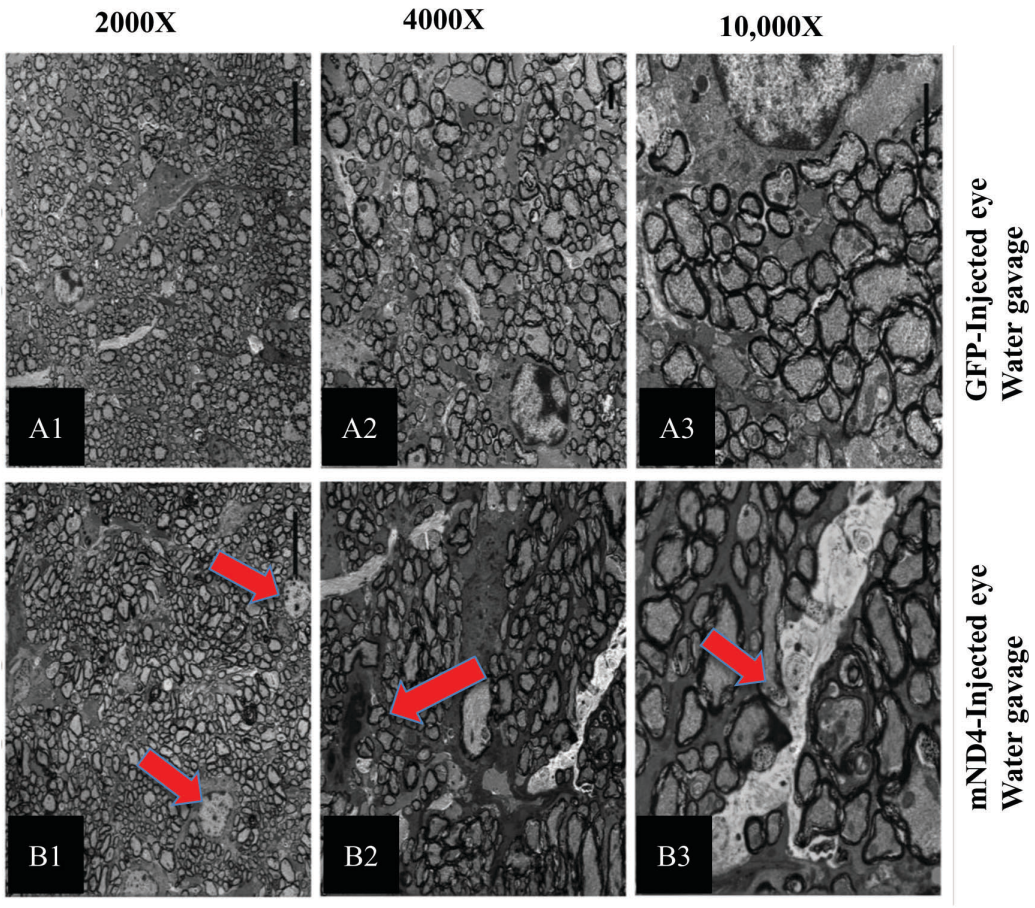

Figure 19. The disease process is not affected by water gavage. A1-A3) Optic nerve of GFP-injected eye shows healthy axons and an absence of glial cell degeneration. B1-B3 (mND4-injected eye) B1) White bodies are non-myelinated axons indicating that oligodendrocytes are beginning to degenerate. B2) the black body (arrow) is an apoptotic glial cell. B3) White large degenerated processes indicating degeneration of glial cells.

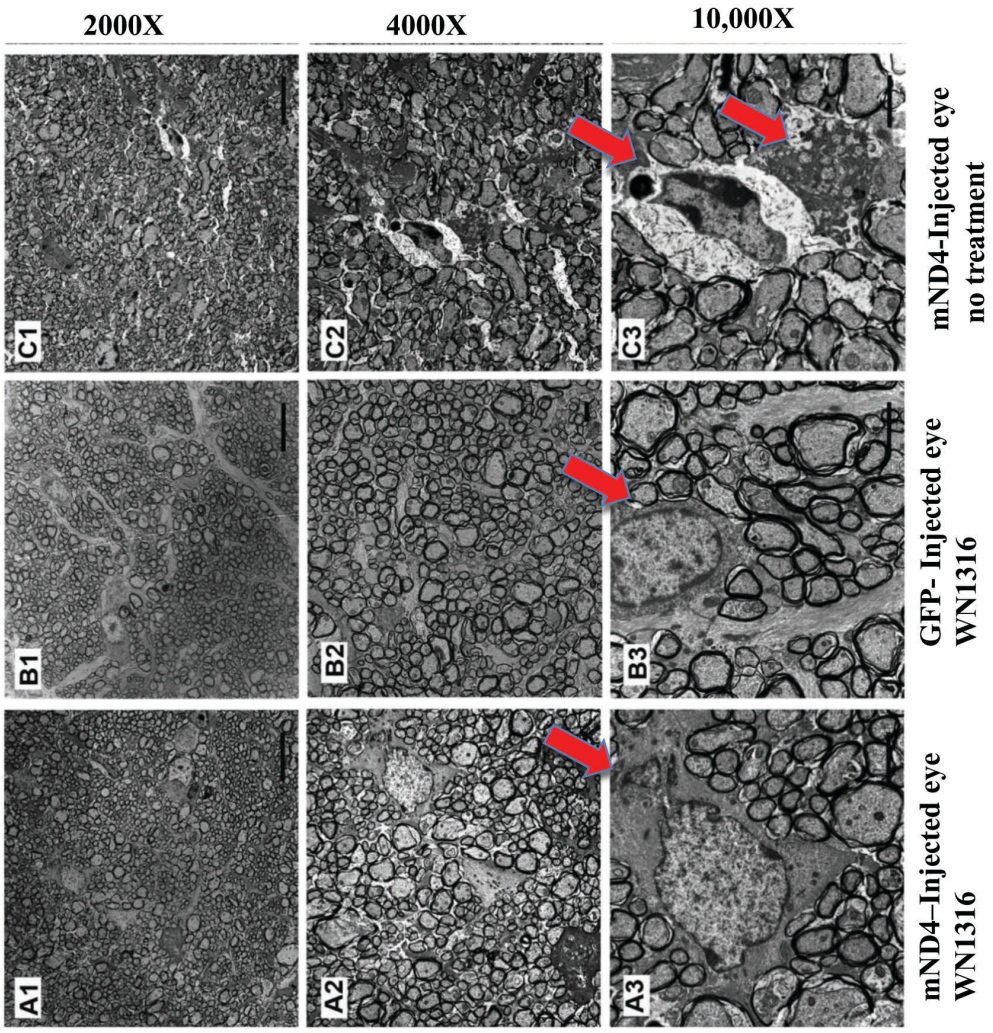

Figure 20. WN1316 appears to slow disease progression. A1-A3) Optic nerve of mND4-injected eye treated with WN1316 shows a large nucleus that is beginning fragmentation (arrow in A3) but is still in much better shape than an mND4-injected eye that received no treatment (C1-C3). This suggests that WN1316 is delaying disease progression. The GFP injected eye in the WN1316 group (B1-B3) has normal processes indicating normal glial cells and normal healthy nuclei.

CHAPTER 4-DISCUSSION

This thesis examined the therapeutic potential of WN1316, a small molecule compound, in the treatment of Leber's Hereditary Optic Neuropathy (LHON), which is a devastating form of blindness with no effective treatment to date. WN1316 had previously been shown to be effective in the treatment of a mouse model of Amyotrophic Lateral Sclerosis (ALS), a rapidly progressive neurological disorder characterised by degeneration of large motor neurons in the cerebral cortex, marked demyelination of fibers in the cervical and lumbar ventral roots and mortality within 3-5 years after diagnosis (Tandan & Bradley, 1985). For both LHON and ALS, the exact mechanism underlying the selective loss of neurons is not clearly understood. However, the two diseases share a common pathological pathway - oxidative stress. Oxidative stress is a deleterious cellular condition in which increased production of free radicals (also referred to as reactive oxygen species [ROS], or decreased cellular anti-oxidant defence can lead to damage to cellular structure, including lipids, proteins and DNA (Valko et al., 2007). Because of the common pathway shared by both ALS and LHON, and due to the effectiveness of WN1316 in preserving motor function and delaying disease progression in ALS, we decided to test it in *in vitro* and *in vivo* models of LHON.

In *in vitro* studies, we tested the effects of WN1316 in protecting SH-SY5Y neuroblastoma cells against the oxidative stressor menadione, and 661W cells against two oxidative stressors: menadione and hydrogen peroxide. In addition, we tested the potential of combination therapy of WN1316 and the (X-linked Inhibitor of Apoptosis protein) XIAP in 661W cells.

Apoptosis and oxidative stress are two important aspects of the complex LHON disease pathology (Ghelli et al., 2003) (Zhuo, Luo, & Zhang, 2012). Activation of the apoptotic cascade in retinal neurons appears to occur via activation of a family of proteins called caspases (mainly caspases 3, 7 and 9) that trigger the cleavage of cellular proteins leading to cell death (Hyman & Yuan, 2012). XIAP is a direct suppressor of the activity of the caspases 3, 7 and 9 and is thus considered one of the most anti-apoptotic proteins. Our previous studies have shown the potent neuroprotective effects of XIAP in various retinal disease models (Renwick et al., 2006) (Leonard et al., 2007) (Zadro-Lamoureux et al., 2009).

We clearly demonstrated that WN1316 has potent protective effects in the two cell lines against oxidative stress-induced cell death with both stressors, and that the combination therapy with XIAP is giving the best neuroprotection. In their study, Tanaka et al. (2014), have shown that 6μM WN1316 selectively protects SH-SY5Y cells against cell death induced by the oxidative stressors, menadione, α-naphthoquinone and 6-hydroxydopamine (6-OHDA); however this effect was not seen by the non-oxidative stressors, staurosporine and okadaic acid. This result obviously identifies WN1316 as a potential and selective protector against oxidative stress-induced damage. As stated, WN1316 neuroprotection is mediated by the activation of Nrf2 anti-oxidant signalling pathway. Nrf2 transcription factor requires ROS for the activation of anti-oxidant molecules HO-1 and NAD(P)H dehydrogenase [quinone] 1 (NQO1 confirming the requirement of intracellular ROS for WN1316 activation of Nrf2 (Tanaka et al., 2014) (Itoh et al., 1999). These results further strengthen the advantage of WN1316 as a novel therapeutic strategy for the treatment of LHON, in which oxidative stress plays a major role.

The research group of John Guy (University of Miami) has generated two animal

models of LHON, both expressing mutant ND4 (Qi, Sun, Lewin, Hauswirth, & Guy, 2007) (Yu et al., 2012. In one model, the mutant gene is allotopically expressed in the nucleus and the mutant protein is imported into the mitochondria using a mitochondrial targeting sequence. In the second model, the viral capsid is modified to target the virus to the mitochondria, where the mutant protein is transcribed and translated in its natural setting. Our studies used the allotopic expression of mutant ND4 to generate the LHON mouse.

In the allotopic model, Qi et al. (2007) showed reduction of retinal ganglion cell function, tested by Pattern Electroretinography (PERG), as fast as one month after mutant gene inoculation. However, in our hands, the model did not show any differences in RGC function even after four months. The ERG analysis at 4 months showed no differences between the mND4-injected and GFP-injected eyes regardless of the treatment group and no differences in function between the different treatment groups. In personal communication with the authors of that study, they revealed that they have seen great variability between animals, which we saw also in our model, and that the reduction in function was seen in only some animals as early as one month while in others it was not seen until after one year. Moreover, they performed structural analyses by spectral domain optical coherence tomography and electron microscopy at one year after disease onset. After personal communication with Dr. Guy and members of his group at the ARVO conference (Seattle, 2016), we believe that the disease did not progress sufficiently in five months to allow loss of RGCs. It is therefore not surprising that measurements of ERGs, optic nerve cross sectional areas, optic nerve diameters and axon counts revealed no differences between disease and control eyes, making it difficult to assess the effects of WN1316 therapy.

Interestingly, WN1316 treatment in both the mND4 and the GFP groups showed a

trend towards improved ERG values compared with water gavage and no treatment (despite the fact that this improvement did not reach significance). Although additional experiments need to be conducted to determine if this effect is real, this finding may suggest that WN1316 is protecting RGCs from the normal loss, which is associated with aging. In fact, depending on the type of species, up to 35-40 % of RGCs can be lost within the life span of the animal (Neufeld & Gachie, 2003) (Wang, Yuan, & Neufeld, 2007). Since our mice were injected at 2 months of age and treated for a further 5 months, they would have been approximately 7 months old at the end of the experiment and should have lost approximately 16% of their RGCs through the aging process.

Electron microscopy (EM) analysis of the optic nerves was the only outcome measure that gave indications of the disease. EM showed signs of advanced nuclear fragmentation, apoptotic cell bodies and numerous white processes. Whereas the disease process was not affected by water gavage, we saw a delay in disease progression shown as decreased apoptosis, slower nuclear fragmentation and more preservation of cellular components only in the WN1316 group. The EM analysis was conducted blindly by Yves de Repentigny (Kothary Lab, OHRI), who was able to correctly identify which of the animals had received mutant ND4 or GFP and which had also received WN1316. These results are promising for the use of WN1316 as a therapeutic strategy in the treatment of LHON. WN1316 is currently in phase I clinical trials in Japan as a potential candidate drug for the treatment of ALS. All toxicity, safety and pharmacokinetics studies have been performed showing a wide range of safety and tolerability, with no reported adverse effects https://upload.umin.ac.jp/cgi-open-bin/ctr_e/ctr_view.cgi?recptno=R000017516). These studies bode well for WN1316 to be easily transferable for the treatment of LHON.

It is obvious from the *in vivo* results of this study that the time point of the animal experiment was not sufficient to see disease progression. In addition, the great variability between animals that we and others have seen are limitations. In future studies, we will expand the time course of the treatment to allow greater time for the progression of the disease. In addition, there is now a transgenic mouse model of LHON (Yu et al., 2015) that provides a bit less variability between animals and is a good alternative to the use of AAV-mediated disease induction.

Future studies:

Mitochondrial diseases have complicated and multifactorial aspects. In these disorders, even if the causative mutation is identified, effective therapies remain elusive. This is mostly due to the unknown mechanisms leading from gene mutation to initiation and progression of disease. Learning more about these disease mechanisms will support the development of targeted therapeutic approaches that will halt cell death and ultimately prevent vision loss. In LHON, to develop anti-apoptotic and anti-oxidative stress therapeutic strategies, it is essential to study the effects of mutations on mitochondrial function. To date, most of studies to understand LHON mutations are obtained from cytoplasmic hybrid (cybrid) cell lines. These cybrids are generated by fusing osteosarcoma cells depleted of their mitochondria with enucleated LHON fibroblasts (Wilkins, Carl, & Swerdlow, 2014) (Levin, 2007). These cybrids will retain their original tumour cell characteristics and remain glycolytic (depending on glycolysis for energy synthesis), whereas neuronal cells, such as RGCs affected in LHON, depend on OXPHOS as the main source of energy (Ghelli et al., 2003). Consequently, cybrids are limited in their ability to give insight into LHON mutations. For this reason, generating primary RGC cultures to study mitochondrial bioenergetics will

be optimal to understand the effects of the ND4 mutation and to evaluate WN1316 therapy in improving mitochondrial function.

In future studies, I will isolate primary RGCs by immunopanning (Winzeler & Wang, 2013) (Winzeler & Wang, 2013). We received a modified protocol for the culture of RGCs from Dr. Wang, which will enable better yield of RGCs from neonatal mice. RGCs should survive for 2-3 weeks in culture, allowing us to conduct biochemical assays to determine the effects of the LHON mutation on mitochondrial function. By injecting newborn pups with AAV-mND4, followed by isolation of RGCs that are expressing the mutant ND4 from 7-14 day old mice, an *in vitro* LHON model can be generated. Assays to measure OXPHOS and glycolysis can then be used to assess mitochondrial function in untreated normal and LHON RGCs.

CHAPTER 5- CONCLUSION

Blindness caused by Leber's Hereditary Optic Neuropathy LHON, although not life threatening, places a huge burden on patients' lives that is without cure to date. Apoptosis and oxidative stress are two main pathways in the pathogenesis of LHON. In previous work, we have shown that XIAP prevents cell death, a main cause of visual loss in various retinal diseases. WN1316 was shown to be effective in an ALS model. In this study, WN1316 protected cells against oxidative stress-induced cell death and combination therapy of XIAP and WN1316 had the best survival outcome in the *in vitro* model. WN1316 also appears to rescue in our *in vivo* model. However, a longer disease timeline and more experiments are needed to further confirm this effect.

REFERENCES:

Abu-Amero, K. K. (2011). Leber's Hereditary Optic Neuropathy: The Mitochondrial Connection Revisited. *Middle East African Journal of Ophthalmology*, *18*(1), 17–23. http://doi.org/10.4103/0974-9233.75880

Alberts, B., Johnson, A., Lewis, J., Raff, M., Roberts, K., & Walter, P. (2002). The Mitochondrion. Retrieved from http://www.ncbi.nlm.nih.gov/books/NBK26894/

Anderson, S., Bankier, A. T., Barrell, B. G., de Bruijn, M. H. L., Coulson, A. R., Drouin, J., Young, I. G. (1981). Sequence and organization of the human mitochondrial genome. *Nature*, *290*(5806), 457–465. http://doi.org/10.1038/290457a0

Battisti, C., Formichi, P., Cardaioli, E., Bianchi, S., Mangiavacchi, P., Tripodi, S. A., Federico, A. (2004). Cell response to oxidative stress induced apoptosis in patients with Leber's hereditary optic neuropathy. *Journal of Neurology, Neurosurgery & Psychiatry*, *75*(12), 1731–1736. http://doi.org/10.1136/jnnp.2003.024372

Bibb, M. J., Van Etten, R. A., Wright, C. T., Walberg, M. W., & Clayton, D. A. (1981). Sequence and gene organization of mouse mitochondrial DNA. *Cell*, *26*(2), 167–180. http://doi.org/10.1016/0092-8674(81)90300-7

Calkins, M. J., Johnson, D. A., Townsend, J. A., Vargas, M. R., Dowell, J. A., Williamson, T. P., Johnson, J. A. (2008). The Nrf2/ARE Pathway as a Potential Therapeutic Target in

Neurodegenerative Disease. *Antioxidants & Redox Signaling*, *11*(3), 497–508. http://doi.org/10.1089/ars.2008.2242

Cleveland, D. W., & Rothstein, J. D. (2001). From charcot to lou gehrig: deciphering selective motor neuron death in als. *Nature Reviews Neuroscience*, *2*(11), 806–819. http://doi.org/10.1038/35097565

Cooper, G. M. (2000). Mitochondria. Retrieved from http://www.ncbi.nlm.nih.gov/books/NBK9896/

De Vries, H. E., Witte, M., Hondius, D., Rozemuller, A. J. M., Drukarch, B., Hoozemans, J., & van Horssen, J. (2008). Nrf2-induced antioxidant protection: A promising target to counteract ROS-mediated damage in neurodegenerative disease? *Free Radical Biology and Medicine*, *45*(10), 1375–1383. http://doi.org/10.1016/j.freeradbiomed.2008.09.001

Ghelli, A., Zanna, C., Porcelli, A. M., Schapira, A. H. V., Martinuzzi, A., Carelli, V., & Rugolo, M. (2003). Leber's Hereditary Optic Neuropathy (LHON) Pathogenic Mutations Induce Mitochondrial-dependent Apoptotic Death in Transmitochondrial Cells Incubated with Galactose Medium. *Journal of Biological Chemistry*, *278*(6), 4145–4150. http://doi.org/10.1074/jbc.M210285200

Giordano, L., Deceglie, S., d'Adamo, P., Valentino, M. L., La Morgia, C., Fracasso, F., Cantatore, P. (2015). Cigarette toxicity triggers Leber's hereditary optic neuropathy by affecting

mtDNA copy number, oxidative phosphorylation and ROS detoxification pathways. *Cell Death & Disease*, *6*(12), e2021. http://doi.org/10.1038/cddis.2015.364

Guy, J., Yu, H., Porciatti, V., Hauswirth, W. W., Chiodo, V., Boye, S. L., & Chou, T.-H. (2012). Mutant ND4 Gene Delivery to Mitochondria by Targeting Sequence-Modified AAV Induces Visual Loss and Optic Atrophy in Mice. *Investigative Ophthalmology & Visual Science*, *53*(14), 3166–3166.

Howell, N. (1997). Leber hereditary optic neuropathy: mitochondrial mutations and degeneration of the optic nerve. *Vision Research*, *37*(24), 3495–3507. http://doi.org/10.1016/S0042-6989(96)00167-8

Hyman, B. T., & Yuan, J. (2012). Apoptotic and non-apoptotic roles of caspases in neuronal physiology and pathophysiology. *Nature Reviews Neuroscience*, *13*(6), 395–406. http://doi.org/10.1038/nrn3228

Itoh, K., Wakabayashi, N., Katoh, Y., Ishii, T., Igarashi, K., Engel, J. D., & Yamamoto, M. (1999). Keap1 represses nuclear activation of antioxidant responsive elements by Nrf2 through binding to the amino-terminal Neh2 domain. *Genes & Development*, *13*(1), 76–86.

Karanjia, R., ten Hove, M. W., & Coupland, S.G. (2011). Electroretinograms and Normative Data. In G. Belusic (Ed.), *Electroretinograms*. InTech. Retrieved from

http://www.intechopen.com/books/electroretinograms/electroretinograms-and-normative-data.

Kirches, E. (2011). LHON: Mitochondrial Mutations and More. *Current Genomics*, *12*(1), 44–54. http://doi.org/10.2174/138920211794520150

Koilkonda, R. D., Guy, J., Koilkonda, R. D., & Guy, J. (2010). Leber's Hereditary Optic Neuropathy-Gene Therapy: From Benchtop to Bedside. *Journal of Ophthalmology*, *2011, 2011*, e179412. http://doi.org/10.1155/2011/179412, 10.1155/2011/179412

Kolb, H. (2003). How the Retina Works. *American Scientist*, *91*(1), 28. http://doi.org/10.1511/2003.1.28

Krishnamoorthy, R. R., Clark, A. F., Daudt, D., Vishwanatha, J. K., & Yorio, T. (2013). A forensic path to RGC-5 cell line identification: lessons learned. *Investigative Ophthalmology & Visual Science*, *54*(8), 5712–5719. http://doi.org/10.1167/iovs.13-12085

Lenaz, G. (2012). Mitochondria and Reactive Oxygen Species. Which Role in Physiology and Pathology? In R. Scatena, P. Bottoni, & B. Giardina (Eds.), *Advances in Mitochondrial Medicine* (pp. 93–136). Springer Netherlands. Retrieved from http://link.springer.com.proxy.bib.uottawa.ca/chapter/10.1007/978-94-007-2869-1_5

Leonard, K. C., Petrin, D., Coupland, S. G., Baker, A. N., Leonard, B. C., LaCasse, E. C., Tsilfidis, C. (2007). XIAP protection of photoreceptors in animal models of retinitis pigmentosa. *PloS One*, *2*(3), e314. http://doi.org/10.1371/journal.pone.0000314

Levin, L. A. (2007). MECHANISMS OF RETINAL GANGLION SPECIFIC-CELL DEATH IN LEBER HEREDITARY OPTIC NEUROPATHY. *Transactions of the American Ophthalmological Society*, *105*, 379–391.

Mailloux, R. J., & Harper, M.-E. (2012). Mitochondrial proticity and ROS signaling: lessons from the uncoupling proteins. *Trends in Endocrinology & Metabolism*, *23*(9), 451–458. http://doi.org/10.1016/j.tem.2012.04.004

Man, P., Turnbull, D., & Chinnery, P. (2002). Leber hereditary optic neuropathy. *Journal of Medical Genetics*, *39*(3), 162–169. http://doi.org/10.1136/jmg.39.3.162

Man, P. Y. W., Howell, N., Mackey, D. A., Nørby, S., Rosenberg, T., Turnbull, D. M., & Chinnery, P. F. (2004). Mitochondrial DNA haplogroup distribution within Leber hereditary optic neuropathy pedigrees. *Journal of Medical Genetics*, *41*(4), e41–e41. http://doi.org/10.1136/jmg.2003.011247

McCulloch, D. L., Marmor, M. F., Brigell, M. G., Hamilton, R., Holder, G. E., Tzekov, R., & Bach, M. (2015). ISCEV Standard for full-field clinical electroretinography (2015 update). *Documenta Ophthalmologica*, *130*(1), 1–12. http://doi.org/10.1007/s10633-014-9473-7

Meyerson, C., Van Stavern, G., & McClelland, C. (2015). Leber hereditary optic neuropathy: current perspectives. *Clinical Ophthalmology (Auckland, N.Z.)*, *9*, 1165–1176. http://doi.org/10.2147/OPTH.S62021

Neufeld, A. H., & Gachie, E. N. (2003). The inherent, age-dependent loss of retinal ganglion cells is related to the lifespan of the species. *Neurobiology of Aging*, *24*(1), 167–172. http://doi.org/10.1016/S0197-4580(02)00059-3

Nikoskelainen, E. K., Marttila, R. J., Huoponen, K., Juvonen, V., Lamminen, T., Sonninen, P., & Savontaus, M. L. (1995). Leber's "plus": neurological abnormalities in patients with Leber's hereditary optic neuropathy. *Journal of Neurology, Neurosurgery & Psychiatry*, *59*(2), 160–164. http://doi.org/10.1136/jnnp.59.2.160

Papa, S., Rasmo, D. D., Technikova-Dobrova, Z., Panelli, D., Signorile, A., Scacco, S., Sardanelli, A. M. (2011). Respiratory chain complex I, a main regulatory target of the cAMP/PKA pathway is defective in different human diseases. *FEBS Letters*. http://doi.org/10.1016/j.febslet.2011.09.019

Pisano, A., Preziuso, C., Iommarini, L., Perli, E., Grazioli, P., Campese, A. F., Giordano, C. (2015). Targeting estrogen receptor β as preventive therapeutic strategy for Leber's hereditary optic neuropathy. *Human Molecular Genetics*, *24*(24), 6921–6931. http://doi.org/10.1093/hmg/ddv396

Qi, X., Sun, L., Lewin, A. S., Hauswirth, W. W., & Guy, J. (2007). The mutant human ND4 subunit of complex I induces optic neuropathy in the mouse. *Investigative Ophthalmology & Visual Science*, *48*(1), 1–10.

Rasool, N., Lessell, S., & Cestari, D. M. (2016). Leber Hereditary Optic Neuropathy: Bringing the Lab to the Clinic. *Seminars in Ophthalmology*, *31*(1-2), 107–116. http://doi.org/10.3109/08820538.2015.1115251

Renwick, J., Narang, M. A., Coupland, S. G., Xuan, J. Y., Baker, A. N., Brousseau, J., Tsilfidis, C. (2006). XIAP-mediated neuroprotection in retinal ischemia. *Gene Therapy*, *13*(4), 339–347. http://doi.org/10.1038/sj.gt.3302683

Sadun, A. A., La Morgia, C., & Carelli, V. (2011). Leber's Hereditary Optic Neuropathy. *Current Treatment Options in Neurology*, *13*(1), 109–117. http://doi.org/10.1007/s11940-010-0100-y

Saraste, M. (1999). Oxidative Phosphorylation at the fin de siecle . (cover story). *Science*, *283*(5407), 1488–1493.

Saszik, S. M., Robson, J. G., & Frishman, L. J. (2002). The scotopic threshold response of the dark-adapted electroretinogram of the mouse. *The Journal of Physiology*, *543*(Pt 3), 899–916. http://doi.org/10.1113/jphysiol.2002.019703

Scapagnini, G., Butterfield, D. A., Colombrita, C., Sultana, R., Pascale, A., & Calabrese, V. (2004). Ethyl Ferulate, a Lipophilic Polyphenol, Induces HO-1 and Protects Rat Neurons Against Oxidative Stress. *Antioxidants & Redox Signaling*, *6*(5), 811–818. http://doi.org/10.1089/ars.2004.6.811

Tan, E., Ding, X.-Q., Saadi, A., Agarwal, N., Naash, M. I., & Al-Ubaidi, M. R. (2004). Expression of cone-photoreceptor-specific antigens in a cell line derived from retinal tumors in transgenic mice. *Investigative Ophthalmology & Visual Science*, *45*(3), 764–768.

Tanaka, K., Kanno, T., Yanagisawa, Y., Yasutake, K., Inoue, S., Hirayama, N., & Ikeda, J.-E. (2014). A Novel Acylaminoimidazole Derivative, WN1316, Alleviates Disease Progression via Suppression of Glial Inflammation in ALS Mouse Model. *PLoS ONE*, *9*(1). http://doi.org/10.1371/journal.pone.0087728

Tandan, R., & Bradley, W. G. (1985). Amyotrophic lateral sclerosis: Part 1. Clinical features, pathology, and ethical issues in management. *Annals of Neurology*, *18*(3), 271–280. http://doi.org/10.1002/ana.410180302

Valko, M., Leibfritz, D., Moncol, J., Cronin, M. T. D., Mazur, M., & Telser, J. (2007). Free radicals and antioxidants in normal physiological functions and human disease. *The International Journal of Biochemistry & Cell Biology*, *39*(1), 44–84. http://doi.org/10.1016/j.biocel.2006.07.001

Van Bergen, N. J., Wood, J. P. M., Chidlow, G., Trounce, I. A., Casson, R. J., Ju, W.-K., Crowston, J. G. (2009). Recharacterization of the RGC-5 retinal ganglion cell line. *Investigative Ophthalmology & Visual Science*, *50*(9), 4267–4272. http://doi.org/10.1167/iovs.09-3484

Wallace, D. C., Singh, G., Lott, M. T., Hodge, J. A., Schurr, T. G., Lezza, A. M., Nikoskelainen, E. K. (1988). Mitochondrial DNA mutation associated with Leber's hereditary optic neuropathy. *Science*, *242*(4884), 1427–1430. http://doi.org/10.1126/science.3201231

Wang, A. L., Yuan, M., & Neufeld, A. H. (2007). Age-Related Changes in Neuronal Susceptibility to Damage. *Annals of the New York Academy of Sciences*, *1097*(1), 64–66. http://doi.org/10.1196/annals.1379.027

Webvision: http://webvision.med.utah.edu/

West, A. P., Shadel, G. S., & Ghosh, S. (2011). Mitochondria in innate immune responses. *Nature Reviews Immunology*, *11*(6), 389–402. http://doi.org/10.1038/nri2975

Wilkins, H. M., Carl, S. M., & Swerdlow, R. H. (2014). Cytoplasmic hybrid (cybrid) cell lines as a practical model for mitochondriopathies. *Redox Biology*, *2*, 619–631. http://doi.org/10.1016/j.redox.2014.03.006

Winzeler, A., & Wang, J. T. (2013). Purification and Culture of Retinal Ganglion Cells from Rodents. *Cold Spring Harbor Protocols*, *2013*(7), pdb.prot074906. http://doi.org/10.1101/pdb.prot074906

Winzeler, A., & Wang, J. T. (2013). Purification and culture of retinal ganglion cells. *Cold Spring Harbor Protocols*, *2013*(7), 614–617. http://doi.org/10.1101/pdb.top070961

Xu, D. G., Crocker, S. J., Doucet, J.-P., St-Jean, M., Tamai, K., Hakim, A. M., Robertson, G. S. (1997). Elevation of neuronal expression of NAIP reduces ischemic damage in the rat hippocampus. *Nature Medicine*, *3*(9), 997–1004. http://doi.org/10.1038/nm0997-997

Yu, H., Koilkonda, R. D., Chou, T.-H., Porciatti, V., Mehta, A., Hentall, I. D., Guy, J. (2015). Consequences of zygote injection and germline transfer of mutant human mitochondrial DNA in mice. *Proceedings of the National Academy of Sciences of the United States of America*, *112*(42), E5689–E5698. http://doi.org/10.1073/pnas.1506129112

Yu, H., Ozdemir, S. S., Koilkonda, R. D., Chou, T.-H., Porciatti, V., Chiodo, V., Guy, J. (2012). Mutant NADH dehydrogenase subunit 4 gene delivery to mitochondria by targeting sequence-modified adeno-associated virus induces visual loss and optic atrophy in mice. *Molecular Vision*, *18*, 1668–83.

Yu-Wai-Man, P., & Chinnery, P. F. (1993). Leber Hereditary Optic Neuropathy. In R. A. Pagon, M. P. Adam, H. H. Ardinger, S. E. Wallace, A. Amemiya, L. J. Bean, K. Stephens (Eds.),

GeneReviews(®). Seattle (WA): University of Washington, Seattle. Retrieved from http://www.ncbi.nlm.nih.gov/books/NBK1174/

Yu-Wai-Man, P., Griffiths, P. G., & Chinnery, P. F. (2011). Mitochondrial optic neuropathies – Disease mechanisms and therapeutic strategies. *Progress in Retinal and Eye Research*, *30*(2-2), 81–114. http://doi.org/10.1016/j.preteyeres.2010.11.002

Zadro-Lamoureux, L. A., Zacks, D. N., Baker, A. N., Zheng, Q.-D., Hauswirth, W. W., & Tsilfidis, C. (2009). XIAP effects on retinal detachment-induced photoreceptor apoptosis [corrected]. *Investigative Ophthalmology & Visual Science*, *50*(3), 1448–1453. http://doi.org/10.1167/iovs.08-2855

Zhuo, Y., Luo, H., & Zhang, K. (2012). Leber hereditary optic neuropathy and oxidative stress. *Proceedings of the National Academy of Sciences of the United States of America*, *109*(49), 19882–19883. http://doi.org/10.1073/pnas.1218953109